

2020

Influence of pH and protein ChePep on motility of *Helicobacter pylori*

<https://hdl.handle.net/2144/39355>

"Downloaded from OpenBU. Boston University's institutional repository."

BOSTON UNIVERSITY
COLLEGE OF ENGINEERING

Thesis

**INFLUENCE OF pH AND PROTEIN CHEPEP ON
MOTILITY OF *HELICOBACTER PYLORI***

by

WENTIAN LIAO

B.E., Nanjing University of Science and Technology, 2018

Submitted in partial fulfillment of the
requirements for the degree of
Master of Science

2020

Approved by

First Reader

Rama Bansil, Ph.D.
Professor *Emerita* of Physics
Professor *Emerita* of Materials Science and Engineering

Second Reader

Soumendra N. Basu, Ph.D.
Professor of Mechanical Engineering
Professor and Associate Division Head of Materials Science and
Engineering

ACKNOWLEDGMENTS

I would like to thank Professor Rama Bansil for her patient and professional instruction. Her professional suggestion and guidance foster me into a better candidate for further research. I shall always remember this wonderful journey working with her.

It has been my pleasure to work in Bansil lab with outstanding students from different discipline, I would like to thank Clover Su for her detailed training and kind help all the time. I would also like to thank Maira Constantino for providing the data and guidance during my analysis and Kasia Bieniek for teaching me rotation analysis. I also what to thank Meaghan Richardson and Yilin Zhu for their kind help and support.

While completing this thesis I was supported by NIH NIGMS R01GM131408 subaward no. 10047369-S1 from Univ. of Utah to Prof. Rama Bansil.

**INFLUENCE OF pH AND PROTEIN CHEPEP ON
MOTILITY OF *HELICOBACTER PYLORI***

WENTIAN LIAO

ABSTRACT

The gastric disease-causing bacteria, *Helicobacter pylori* utilize flagella driven motility and chemotaxis to detect external acidic signal as they cross the pH gradient in the viscoelastic, gel-like mucus layer. The first part of this work explores the effects of pH on *H. pylori*'s motility in both culture broth (BB10) and porcine gastric mucin (PGM). In the human stomach there is a pH gradient across the gastric mucus layer, varying from pH 2 on the luminal surface to pH 7 on the epithelial surface. Both the flagellar motor and viscoelastic properties of medium depend on the pH, thus the change of motility of *H. pylori* across a pH gradient is complicated. The data from experiments performed by Dr. C. Su of the Bansil lab were analyzed and torque was calculated using resistive force theory (RFT). The results indicated that decreasing pH leads to decreased fraction of motile trajectories and mainly impacts the high end of distributions of swimming speeds and length of trajectories. At all pH's the bacteria swim faster and have longer trajectory lengths in BB10 as compared to PGM. While bacteria are stuck in PGM gels at low pH's, they swim at low pH in broth, albeit with reduced speed. The body rotation rate and estimated cell body torque are weakly dependent on pH in BB10, whereas in PGM the bacteria stuck in the low pH gel rotate faster than the motile bacteria leading to increased torque below pH 4. The second part of this thesis explores the influence of the protein ChePep on the motility on *H. pylori*. Based on the movies recorded by Dr. M.

Constantino also of the Bansil lab, a detailed motility comparison and torque estimation between wild type (WT) *H. pylori* and a mutant lacking ChePep (Δ ChePep) were performed. The mutant Δ ChePep shows higher reversal frequency but similar rotation rate as compared with WT. The drastic increase of reversal frequency in Δ ChePep reveals the malfunction of chemotaxis system of Δ ChePep whose flagellar rotation are over-active.

TABLE OF CONTENTS

ACKNOWLEDGMENTS	iv
ABSTRACT.....	v
TABLE OF CONTENTS.....	vii
LIST OF TABLES	x
LIST OF FIGURES	xi
Chapter 1: Introduction.....	1
1.1 The Survival and Colonization of <i>Helicobacter pylori</i>	1
1.2 Chemotaxis	2
1.3 Run-reverse-reorient Motility of <i>H. pylori</i>	2
1.4 Low Reynolds Number Swimming	3
1.5 Resistive Force Theory	4
Chapter 2: Materials and Methods.....	6
2.1 Materials and Experimental Techniques.....	6
2.2.1 Trajectory Segmentation.....	6
2.2.2 Single Cell Tracking	8
2.2.3 Cell Body Rotation Frequency and Cell Body Parameters Measurement	9
2.2.4 Statistics Methods	10
2.2.5 Resistive Force Theory	12
Chapter 3: Effects of pH on Motility of <i>H. pylori</i> in BB10 and PGM	14

3.1 Abstract	15
3.2 Introduction	15
3.3 Results	20
3.3.1 <i>Microrheology of BB10 and PGM</i>	20
3.3.2 <i>Confocal Imaging of PGM Reveals a Heterogeneous Structure at Low pH ...</i>	25
3.3.3 <i>pH Dependence of Swimming Speed Distributions of <i>H. pylori</i> in BB10 and PGM</i>	25
3.3.4 <i>The Effect of pH on Cell Body Rotation in BB10 and PGM</i>	34
3.3.5 <i>Estimation of Torque using Resistance Force Theory (RFT)</i>	39
3.3.6 <i>Different Types of Stuck Bacteria</i>	43
3.4 Discussion	44
3.5 Conclusions	48
Chapter 4: Influence of ChePep on Motility of <i>H. pylori</i>	50
4.1 Abstract	50
4.2 Introduction	51
4.3 Results	55
4.3.1 <i>Super-Diffusive Behavior of Bacteria</i>	55
4.3.2 <i>Motility Analysis of WT and ΔChePep <i>H. pylori</i></i>	58
4.3.3 <i>Body Rotation Analysis of WT and ΔChePep <i>H. pylori</i> and Resistive Force Theory</i>	65
4.4 Discussion	68
4.5 Conclusions	71

Supplementary Information	72
Bibliography	77
CURRICULUM VITAE.....	87

LIST OF TABLES

Table 4. 1 Mean, standard deviation, skew, median and mode of the average run speeds (v_{run}) and reorientation angle (θ_{re}) of <i>H. pylori</i> swimming in BB10.....	59
Table 4. 2 p-value of K-S statistics test of the raw data of t_{run} , d_{run} , v_{run} , θ_{run}	61
Table 4. 3 The parameters of a gamma function fit to the probability distribution data for t_{run} shown in Fig. 3.4. 2, where $P_t, a, \lambda = \lambda t^{a-1} e^{-\lambda t} / \Gamma(a)$	65
Table. S1 Summary of 2 peak fit. The parameters of the 2 Gaussian peaks for v_{inst} and v_{run} speed distributions in PGM and BB10 at different pH. The fit function is given in Methods and width = $\sqrt{2} \sigma$	76

LIST OF FIGURES

Figure 1. 1 Phase contrast image of wild-type *H. pylori* LSH100 in PGM taken with 100X oil immersion lens. The contour (blue) and the centerline (red) obtained with CellTool^{®29} are superimposed in the image. Figure adapted from⁷.....8

Figure 1. 2 Measuring the shape parameters of the body. (A) End-to-end axial length of the body (X_B) in black. (B) Sine fit of centerline in black, where the first 4 and last 4 points of centerline were not considered for the fitting. Figure adapted from Constantino thesis 2017.²¹9

Figure 3. 1 Microrheology of BB10 and PGM at various pHs. (A) Average mean-square displacement ($\langle MSD \rangle$) of BB10 (hollow symbols), PGM (filled symbols) at pH 2 - 7 averaged across all particles. (B) Bar graphs of the exponent α versus pH calculated from $\langle MSD \rangle$ of all particles. (C) HR and viscosity η of BB10 and 15 mg/ml PGM calculated as discussed in the text. The arrows in (C) point towards the respective axes. The microrheology data for PGM is reproduced from ref¹⁸ with permission of author.23

Figure 3. 2 Images of trajectories in BB10 (A) and PGM (B) at different pHs as indicated.....28

Figure 3. 3 The distribution of trajectory displacements in BB10 (A) and PGM (B) at different pH's as indicated, and the dependence of the average displacement (mean and median) with pH in BB10 (C) and PGM (D). Note that trajectories with $d < 4 \mu m$ are not displayed as these correspond to bacteria which are immotile and only display passive Brownian motion.....29

Figure 3. 4 Distributions of swimming speeds and turn angles of *H. pylori* J99 strain in BB10 and PGM at various pH. Histograms summarizing the instantaneous speed (v_{ins}) (no color) and the run speed (v_{run}) distributions (blue) in BB10 (**A**) and PGM (**B**) are shown at different pHs as indicated. When the two histograms overlap the outline of the v_{ins} histogram is visible over the blue histogram. The average speeds (mean and median) for $\langle v_{ins} \rangle$ and $\langle v_{run} \rangle$ and standard deviation (σ) as a function of pH in BB10 and PGM are shown in **C** and **D**. The turn angle (θ_{re}) distributions of J99 WT in BB10 (**E**) and in PGM (**F**) at different pH as indicated.....34

Figure 3. 5 Rotation of cell body as the bacterium swims. (A) A series of frames showing the image of a single bacterium at 100X as it rotates while translating in BB10 at pH 4. (B) A typical contour and the center line obtained from CellTool . (C) Successive contours along the bacterium’s trajectory. The points A, B, C, D indicate reorientation events as described in the text. The frames shown in (A) are from the motion segment, A to B. (D) Alignment angle (with reference to an arbitrary direction) showing oscillations as the cell rotates. The movie for this data are obtained from Su dissertation³²35

Figure 3.6 The bubble plots in E, F, G, H, I, J show cell body rotation rate (Ω) of J99 in BB10 (E) and PGM (F), the ratio V/Ω in BB10 (G) and PGM (H), estimated cell body torque T_c in BB10 (I) and PGM (J), and motor torque T_m in BB10 (K) and PGM (L) calculated as described in the text for all of the bacteria imaged at pH 3 to 6. Note that T_m was not calculated for stuck bacteria for reasons discussed in the text . Cell body torque is plotted as T_c / η and motor T_m is plotted as $T_m / (100 \eta)$. The

mean and standard deviation are indicated. The dashed lines are a guide to the eye. The gray shaded region represents the pH range over which PGM gels and bacteria did not translate but only rotated37

Figure 3.7 Phase contrast microscopic time-lapse montages and trajectories of various modes of bacteria stuck in PGM at low pH. **(A)** Bacterium appears to rotate about a fixed point (indicated by the red x) with fast and slow body rotation rate over time. **(B)** Bacterium moves in a fixed circular trajectory perhaps reflecting proximity to a region of high PGM concentration (dark region) Time increases going clockwise through the images. **(C)** Bacterium at pH 4.5 in PGM showing rotations along with small, random translational displacements. **(D)** Bacterium in BB10 at pH 4 shows a clear translation while rotating. The scale bars in **A-D** indicate a length of 2.5 μm . The images in **E, F, G, H** are overlays of different frames of the movie onto a single image to show the trajectory corresponding to **A, B, C, D** respectively, with the green arrows indicating the direction of motion. The movies for this data are provided in Su dissertation³².43

Figure 4. 1 (A) (B) Trajectories for ΔChePep with reversal and WT without reversal respectively. **(C) (D)** Reorientation angle versus time for ChePep with reversal and WT without reversal respectively where the red circle indicates reversal event57

Figure 4. 2 (A) Analysis of MSD vs. time of all trajectories in BB10. Black dash lines are reference lines for $\alpha = 1$ and $\alpha = 2$ **(B)** Smooth histogram of the α distribution of all trajectories of WT (red) and ΔChePep (black)57

Figure 4. 3 (A) Smooth histogram of run time distribution of WT (red) and Δ ChePep(black) (B) Smooth histogram of displacement per run distribution of WT (red) and Δ ChePep(black) (C) Smooth histogram of run speed distribution for WT (red)with less reversal and ChePep (black)with more reversal respectively (D) Smooth histogram of the reorientation angle distribution of all trajectories of WT (red) and Δ ChePep (black).....58

Figure 4. 4 (A) (B) Smooth histogram of relative speed difference of Δ ChePep (in black) and WT (in red) respectively. The blue dash line is three gaussian peaks of smooth histogram. (C) Smooth histogram of relative reorientation difference of Δ ChePep (in black) and WT (in red) respectively62

Figure 4. 5 (A) (C) Estimated probability density function of reorientation angle (θ) versus δV of WT and Δ ChePep respectively. (B) (D) Contour of probability density function of reorientation angle (θ) versus δV of WT and Δ ChePep respectively.63

Figure 4. 6 (A) (B) Histogram of reorientation angle (θ) distribution whose δV is in the range of -0.2 to 0.2 for Δ ChePep (in black) and WT (in red) respectively.....64

Figure 4. 7 (A) Scatter plot of the cell body rotational rate (Ω) for WT (in red) and Δ ChePep (in black) respectively. (B) Scatter plot of the translational speed (V) for WT (in red) and Δ ChePep (in black) respectively. (B) Scatter plot of the V/Ω for WT (in red) and Δ ChePep (in black) respectively. (D) Scatter plot of cell body torque for WT (in red) and Δ ChePep (in black) respectively. (E) Scatter plot of motor torque for WT (in red) and Δ ChePep (in black) respectively**Error! Bookmark not defined.**

Figure S1 A All particle MSD vs delay time in BB10 at different pHs as indicated. The average $\langle \text{MSD} \rangle$ and relative error of log MSD defined as $\varepsilon = \pm 0.436 \sigma_{\text{MSD}} / \langle \text{MSD} \rangle$ are displayed by the black line and error bars. Numbers in parenthesis on pH legends indicate number of particles tracked.72

Figure S1 B. All particle MSD vs delay time in PGM at different pHs as indicated on a log-log plot. The average $\langle \text{MSD} \rangle$ and relative error of log MSD defined as $\varepsilon = \pm 0.436 \sigma_{\text{MSD}} / \langle \text{MSD} \rangle$ are displayed by the black line and error bars. Numbers in parenthesis on pH legends indicate number of particles tracked.73

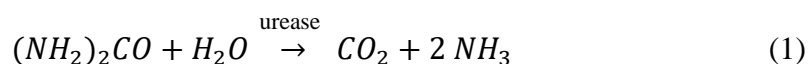
Figure S2 Confocal DIC microscopy images of PGM solution at pH 6 and gel at pH 3. (A) Images at 20X and 40X objective magnifications at pH 6 and 3. The mucin strands are displayed as bright green to blue on the aqueous background indicated by low intensity regions colored in red (see color scale bar on top right). The arrows in the 20X image of PGM at pH3 point to liquid regions with little mucin. (B) The intensity profile measured across the image along the line indicated in yellow in (A).74

Figure S3 Two peak fit of distribution of instantaneous speeds, v_{inst} for J99 *H. pylori* bacteria swimming in BB10 and PGM at different pHs as indicated. The number of motile trajectories that were analyzed ranges from 185 at pH 4 to 388 at pH 3 in BB10 and from 136 at pH 4 to 625 at pH 4.5 in PGM. 75

Chapter 1: Introduction

1.1 The Survival and Colonization of *Helicobacter pylori*

Helicobacter pylori (*H. pylori*) the bacteria that infects more than 50 percent of the total human population¹ are responsible for diseases including gastritis, gastric ulcers and even gastric cancer. Their survival in harsh environment of human stomach depends on its ability to change surrounding pH and chemotactic motility as well as other biochemical and immunological factors. The pathway of *H. pylori* has not been fully understood but it is believed through oral-oral, gastric-oral or fecal-oral contact between person to person at the early childhood. Unlike other bacteria which can not survive in the harsh environment of human stomach due to the secretion of hydrochloric acid in the stomach, *H. pylori* can survive in human stomach, penetrating the protective gastric mucus layer and finally colonize at gastric epithelium surface. Firstly, *H. pylori* can secrete urease which catalyzes the hydrolysis of urea to produce ammonia which will eventually neutralize acid and increase the pH value^{2,3,4}.



Previous work from the Bansil group, Celli *et al.*⁵, has shown that *H. pylori* are unable to translate even though their flagella rotate when they are in a low pH mucin gel (pH < 4) in the absence of urea. Furthermore, they showed that the increase of pH in the presence of urea triggers a gel-sol transition in the gastric mucin gel creating a liquid environment for *H. pylori* to swim in⁶ and penetrate the protective mucus layer and finally colonize at the gastric epithelium surface.

1.2 Chemotaxis

Chemotaxis plays a critical role for the survival of *H. pylori* in the harsh environment of human stomach. *H. pylori* need to distinguish and escape from the low pH environment and further redirect to gastric epithelium surface which is at neutral pH using pH sensitive chemoreceptors^{7,8,9}. Numerous proteins are involved in this process. First, external pH signals are recognized by chemoreceptor protein TlpB which usually localize at bacterial pole^{10,11}. Chemoreceptor proteins then interact with signaling proteins to amplify the signals¹² and transmit the signal into CheAY through proteins CheW or CheV. CheAY triggers the phosphorylation of response regulator CheY^{13,14}. Phosphorylated CheY (CheY-P) interacts with flagellar motor and changes the flagellar rotational direction leading the change of bacterial swimming direction. In order to be continuously responsive for external dynamic signal, phosphorylated CheY needs to return to non-phosphorylated state. The dephosphorylation of protein CheY, thus, is vital for the survival of *H. pylori* in a dynamically acidic environment. The dephosphorylation of CheY can either be achieved by its own auto-dephosphorylation or with the help of phosphatases¹⁵. The most-studied phosphatase is CheZ whose localization depends on ChePep. Thus, protein ChePep are thought to improve the dephosphorylation of CheY^{16,17}. Experiments have shown that Δ ChePep shows a 25% decreased colony diameter in agar plate and 11 times greater reversal frequencies than WT¹⁵ in solution.

1.3 Run-reverse-reorient Motility of *H. pylori*

The run-reversal-reorientation model^{18,19,20} is used to describe the motion of *H. pylori* in this thesis. *H. pylori* has multiple flagella at one pole of its cell body²¹ which can form a

single flagellar bundle. The counterclockwise rotation of flagella bundle will provide a propulsion to push bacteria forward. The clockwise rotation of flagella bundle will pull bacteria backward. Exactly how the transition from forward to reverse motion occurs is a question of considerable interest. One hypothesis is that between the transition of flagellar bundle rotation direction, flagellar bundle needs to de-bundle first. De-bundling may start from the clockwise rotation of one flagellum of the flagellar bundle causing split of flagellar bundle. When all the flagella start to rotate in the same clockwise rotation direction, a new clockwise rotation bundle formed and bacterial swimming direction changes²². Another possibility is that flagella alter their direction by having a flexible hook, and can even flip their direction, wrapping around the body as has been observed in *H. suis* bacteria²³. For some monotrichous bacteria a run-flick-reverse strategy has been observed²⁴. The trajectories exhibit characteristics of a random walk at long-time scales and this has been explained by the run-tumble model developed by Berg²². In tumble state, without uniform flagellar rotation, little propulsion is provided by flagellar motor. However, the translational and rotation diffusion can cause slight displacement and body orientation difference. Berg also founded that by increasing tumble rate, *E. coli* could change their swimming direction more actively to explore a more nutritional environment²⁵.

1.4 Low Reynolds Number Swimming

The Navier-Stokes equations which describes the motion of incompressible viscous fluid is given by

$$\rho \frac{\partial v}{\partial t} + \rho(v \cdot \nabla)v = -\nabla p + \eta \nabla^2 v \quad (2)$$

where v is the velocity field, p is the pressure applied. The left side of the equation is inertial part representing the acceleration of the fluid while the right of the equation is a pressure gradient and viscous drag term. Reynold Number, Re , is the ratio of inertial term $\varphi(v \cdot \nabla)v$ and viscous term $\eta \nabla^2 v$. Thus, for an object with a body size of L with a steady a flow velocity (or rate) of U , the Reynolds number is calculated as $Re =$

$$\frac{\varphi(v \cdot \nabla)v}{\eta \nabla^2 v} = \frac{\varphi L U}{\eta}.$$

For a 10^{-6} m size bacteria swimming in water with a viscosity of 1 cp in the speed of 10^{-6} m/s, the Reynolds number is 10^{-6} which is much smaller than one²⁶. In low Reynolds number region, viscous term dominates and Re could be consider as 0. Equation (2) simplifies to

$$-\nabla p + \eta \nabla^2 v = 0 \quad (3)$$

Thus, the total net force and torque acting on an object swimming in a low Re region will always be zero²⁷.

1.5 Resistive Force Theory

Resistive Force Theory states that at low at low Reynolds number a rotating flagellum produces an axial thrust F and torque T which can be decoupled and is related to the flagellum's axial velocity V and rotation rate Ω ²⁸.

$$\begin{pmatrix} F \\ T \end{pmatrix} = \begin{pmatrix} A_{11} & A_{12} \\ A_{12} & A_{22} \end{pmatrix} \begin{pmatrix} V \\ \Omega \end{pmatrix} \quad (4)$$

where the 2x2 matrix depends on the geometric parameters of the cell body or flagella.

For helical body shape, $T = A_{12}V + A_{22}\Omega$ where A_{12} is the translational drag coefficient

(α) and A_{22} is the rotational drag coefficient (β). For ellipsoidal body shape, $T = A_{22}\Omega$

since A_{12} vanish. Cell body torque and flagellar torque could be estimated from ellipsoidal or helical body parameters and rotation and translational speed recorded from CellTool[®] 29 analysis.

Due to the balance of flagellar torque and motor torque at low Re ³⁰, we could estimate motor torque from flagellar torque.

$$F_c + F_f = 0 \quad (5)$$

$$T_c - T_m = 0 \quad (6)$$

$$T_f - T_m = 0 \quad (7)$$

However, limitation of RFT exist due to its assumption of decoupling, torque balance and the assumption that cell body and flagellar bundle are colinear. A more reliable torque estimation could be done through Regularized Stokeslet model³¹.

Chapter 2: Materials and Methods

All data analysis methods are presented in this chapter. This includes poly-particle tracking, trajectory segmentation, single particle tracing, rotational analysis, statistics analysis and torque estimation. All the data used for analysis were acquired by Prof. Bansil's previous students Clover Su, Maira Constantino and Katarzyna Bieniek.

2.1 Materials and Experimental Techniques

The experiments and data acquisition are performed by Clover Su, Katarzyna Bieniek Maira Constantino and are full discussed in Su 2019³².

2.2 Methods

2.2.1 Trajectory Segmentation

To analyze the motility of *H. pylori*, MATLAB program Poly-particle Tracker is implemented to track the position of each bacteria in recorded movies, as described in³⁴.

With the position $\vec{r}(t) = x(t)\hat{e}_x + y(t)\hat{e}_y$ of each bacterium at each frame, both the position vector and angle vector of bacteria are calculated according $\vec{v}(t)$ and $\vec{\varphi}(t)$ where τ ($\tau = 1/fps$) is the time interval between two consecutive frames and fps is the frame rate.

$$\vec{v}(t) = \frac{\vec{r}(t + \tau) - \vec{r}(t)}{\tau} \quad (8)$$

$$\vec{\varphi}(t) = \arctan\left(\frac{v_y(t)}{v_x(t)}\right) \quad (9)$$

The identification is achieved through the location of large changes in large alignment angle change $|\Delta\varphi|$ and/or the minimum of instantaneous speed V by equation (10) and (11)

$$|\Delta\phi(t_{max})| > \gamma\sqrt{2D_{rot}\tau} \quad (10)$$

$$\text{Max}(|v(t_{min} + \tau) - v(t_{min})|, |v(t_{min} - \tau) - v(t_{min})|) > \beta v(t_{min}) \quad (11)$$

where t_{max} is the time at which $|\Delta\phi|$ is maximum; t_{min} is the time at which v is minimum; $\tau = 0.03\text{s}$ is the time between frames; γ is a threshold variable that determines how much larger than the angular deviation ($\sqrt{2D_{rot}\tau}$) that $|\Delta\phi(t_{max})|$ has to be; and β is a threshold variable that determines how much larger than $v(t_{min})$ that the speed change has to be to be considered a reorientation event. We estimated the rotational diffusion constant D_{rot} of a bacterium by approximating it as an ellipsoid with semi-minor axis $a \approx 0.5 \mu\text{m}$ and semimajor axis $b \approx 1.5 \mu\text{m}$,

$$D_{rot} = \frac{k_B T (\ln(\frac{2b}{a}) - 0.5)}{8\pi\eta b^3/3} \approx 0.2 \text{ rad}^2/\text{s} \quad (12)$$

Using this rotational diffusion constant and by locating $v(t_{min})$ we found $\gamma = 8.5$ and $\beta = 1.75$ to be sufficient to identify reorientations events where bacteria actively reoriented their swimming direction. The bacterium was assumed to stay in the reorientation state for a time t_{re} calculated by examining if the local angle changes $|\Delta\phi(t_{max}+t_{re})|$ was large compared to the $|\Delta\phi(t_{max})|$ and if the displacement of the bacterium was smaller than that of Brownian motion, using the criterion:

$$||\Delta\phi(t_{max})| - |\Delta\phi(t_{max} + \Delta t)|| > \Gamma |\Delta\phi(t_{max})| \quad (13)$$

$$(\mathbf{r}(t_{min} + \Delta t) - \mathbf{r}(t_{min}))^2 < 4D\Delta t \quad (14)$$

where $D = k_B T \frac{\ln(2b/a)}{6\pi\eta b}$ is the translational diffusion of an ellipsoid doing Brownian motion and Γ is the percentage change in angle for which the bacterium is still considered to be in reorientation event. We found that $\Gamma = 0.7$ made the best identification. For H .

pylori $D = 0.26 \mu\text{m}^2/\text{s}$. Reorientation angles between runs are denoted by θ_{re} and if larger than 140° they were identified as reversals.

2.2.2 Single Cell Tracking

To accurately measure the cell body rotation frequency and cell body parameters, movies at 100X magnification and 100 fps are recorded. The trajectory of each motile bacterium is manually selected and cropped using ImageJ^{®35}. Each cropped trajectory is then analyzed separately by CellTool^{®29} to obtain its cell body geometric parameters, body rotation rate and translational speed. CellTool^{®29} analyzes selected and cropped bacteria trajectory one by one. With the movies of each trajectory as input files, CellTool^{®29} first extracts and saves all non-aligned contours and centerlines after which it saves the mean body diameter and centroid position of all consecutive images. Then, aligned contours and centerlines are extracted and alignment angle of all images of each trajectory is saved.

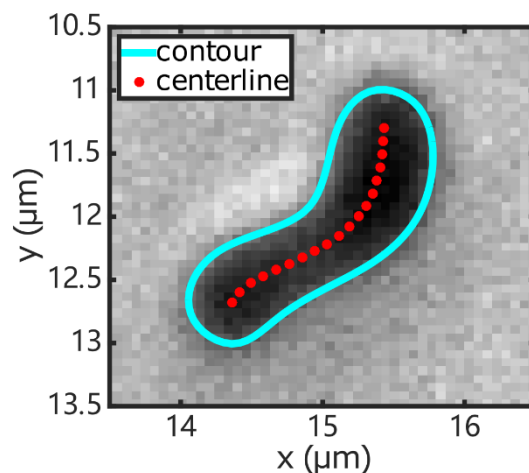


Figure 1. 1 Phase contrast image of wild-type *H. pylori* LSH100 in PGM taken with 100X oil immersion lens. The contour (blue) and the centerline (red) obtained with CellTool^{®29} are superimposed in the image. Figure adapted from³⁶.

2.2.3 Cell Body Rotation Frequency and Cell Body Parameters Measurement

MATLAB programs were used for measuring the cell body parameters. In Figure. 1.2. A, the aligned contours of each image were used to calculate the end-to-end axial length (X_B) which is defined as the distance between two contour points at $y=0$ of the aligned contour. In Figure. 1. 2 B, the most in-focus aligned contour which gives the biggest X_B was selected for the calculation for the resting body parameters including helical pitch (P) and helical radius (R). To obtain the helical geometric body parameters, most in-focus aligned centerline without the end caps of *H. pylori* was fitted using a sine function $y = R \sin(2\pi x/P + \delta)$ where δ allows the sine function to have a phase shift²¹.

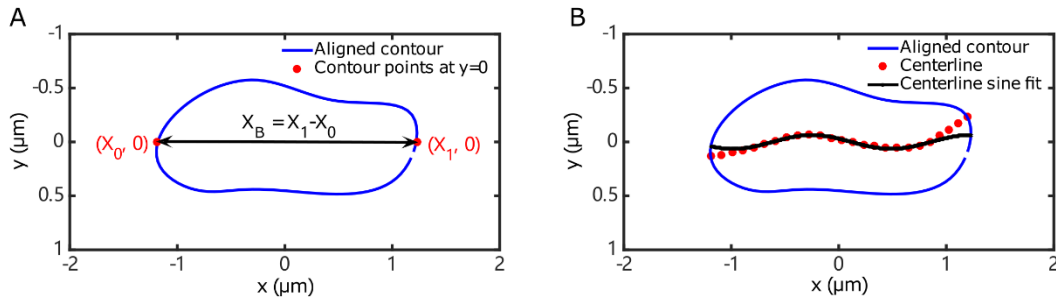


Figure 1.2 Measuring the shape parameters of the body. (A) End-to-end axial length of the body (X_B) in black. (B) Sine fit of centerline in black, where the first 4 and last 4 points of centerline were not considered for the fitting. Figure adapted from Constantino thesis 2017²¹.

The body parameters data were then used to estimate cell body torque and motor torque. At 100X magnification the depth of focus is shorter than that of 40X, which will reduce the time of each bacterium in focus. Higher frame rate will also increase the load of camera, which further limits the length of movies and thus the time of each bacterium in

focus. Fluorescent imaging of GFP could be utilized as a complementary imaging method of phase contrast microscopy as proposed by Constantino²³.

2.2.4 Statistics Methods

2.2.4.1 Kolmogorov-Smirnov Test

We use two-sample Kolmogorov-Smirnov test to examine whether the run speeds of bacteria in different pH comes from the same continuous distribution. Briefly, two-sample Kolmogorov-Smirnov test is a nonparametric hypothesis test which evaluates the difference between the cumulative distribution functions (cdfs) of the distributions of two sample data. The test uses the maximum absolute difference between the cdfs of the distributions of two sample data by

$$D^* = \max(|\hat{F}_1(x) - \hat{F}_2(x)|) \quad (15)$$

where $\hat{F}_1(x)$ is the proportion of x_1 values less than or equal to x and $\hat{F}_2(x)$ is the proportion of x_2 values less than equal to x . The critical value D^* is determined by the significance level α and the number of data points according to K-S test p-value table. We selected 0.05 significance level and the data points varies with different pHs³⁷.

2.2.4.2 Kernel Smoothing Function

The smooth histogram are smoothed by Kernel Smoothing function in MATLAB. The function returns a probability density estimate, f , for each raw data. The estimation is based on a Kernel function which is a nonparametric representation of the probability density function (pdf) of a random variable (raw data). For any real values x from raw data, the kernel density estimator's formula is given by

$$\hat{f}_h(x) = \frac{1}{nh} \sum_{i=1}^n K\left(\frac{x - x_i}{h}\right) \quad (16)$$

where x_1, x_2, \dots, x_n are random samples from an unknown distribution. n is the sample size, $K(\bullet)$ is the kernel smoothing function, and h is the bandwidth³⁸.

2.2.4.3 Exponential Modified Gaussian Fitting

Run speed distribution is fitted into exponential modified gaussian fitting using³⁹

$$y = \frac{h\sigma}{\tau} \sqrt{\frac{\pi}{2}} \exp\left[\frac{(\sigma^2/\tau - 2(x-\mu))}{2\tau}\right] \left[1 + \operatorname{erf}\left(\frac{x-\mu-\sigma^2/\tau}{\sqrt{2}\sigma}\right)\right] \quad (17)$$

Mean, std, skew mode and median are further calculated as follows

$$\text{mean} = \mu + \tau \quad (18)$$

$$\text{std} = \sqrt{\sigma^2 + \tau^2} \quad (19)$$

$$\text{skew} = \frac{2\tau^3}{(\sigma^2 + \tau^2)^{3/2}} \quad (20)$$

$$\text{mode} = \mu^2 + \frac{\sigma^2}{\tau} - \operatorname{sgn}(\tau)\sqrt{2}\sigma \operatorname{erfcxinv}\left(\frac{|\pi|}{\sigma} \sqrt{\frac{2}{\pi}}\right) \quad (21)$$

and median is the middle value of EMG function distribution.

2.2.4.4 Multiple Gaussian Peaks Fitting

The relative speed difference curves for both WT and Δ ChePep were fit to a sum three Gaussians using

$$y = a_{ma} e^{-\left(\frac{x_{ma}-b_{ma}}{c_{ma}}\right)^2} + a_{mi1} e^{-\left(\frac{x_{mi1}-b_{mi1}}{c_{mi1}}\right)^2} + a_{mi2} e^{-\left(\frac{x_{mi2}-b_{mi2}}{c_{mi2}}\right)^2} \quad (22)$$

where a, b, c denotes the amplitude, position and width of the major (ma) and minor (mi) peaks. Note that the width c is equal to $\sigma\sqrt{2}$, where σ is the standard deviation of the Gaussian distribution.

2.2.5 Resistive Force Theory

At low Reynolds number, the motor torque must balance the flagellar torque: $T_m - T_f = 0$ ⁶⁰. Thus, the motor torque T_m could be estimated from flagellar torque T_f which can be estimated from bacterial translational speed v_h and shape factor S_h ¹⁸

$$T_m = v_h/S_h \quad (23)$$

where S_h is calculated from the following equations when consider both cell body and flagellar bundle as helix.

$$S_h = \frac{\frac{\gamma_c}{\beta_c} + \frac{\gamma_f}{\beta_f}}{\alpha_c + \alpha_f - \frac{\gamma_c}{\beta_c} \gamma_c - \frac{\gamma_f}{\beta_f} \gamma_f} \quad (24)$$

where c denotes helical cell body with helical pitch λ_c , radius of helical filament a_c , helical radius R_c , pitch angle φ_c given by $\tan \Phi_c = 2\pi R_c / \lambda_c$, helical contour length $L_c = X_L / \cos \Phi_c$, where X_L is the axial length of cell body. The hydrodynamic translational, rotational and propulsion drag coefficients for the cell body, related to the local normal and tangential force C_n, C_t are given below²⁸:

$$\alpha_c = (C_n \sin^2(\Phi_c) + C_t \cos^2(\Phi_c))L_c \quad (25)$$

$$\beta_c = (C_n \cos^2(\Phi_c) + C_t \sin^2(\Phi_c))R_c^2 L_c \quad (26)$$

$$\gamma_c = (C_n - C_t) \sin(\Phi_c) \cos(\Phi_c) R_c L_c \quad (27)$$

$$C_n = \frac{4\pi\eta}{\ln\left(\frac{2\lambda_c}{a_c}\right) + 1/2} \quad (28)$$

$$C_t = \frac{2\pi\eta}{\ln\left(\frac{2\lambda_c}{a_c}\right) - 1/2} \quad (29)$$

Here η denotes the viscosity of the medium. By changing the subscript c to f these equations give the same quantities for the flagella helix in terms of its helical parameters. The flagella parameters that we used were same as Constantino *et al.*³⁶: $X_f = 2.97 \mu\text{m}$, $a_f = 0.07 \mu\text{m}$, $\lambda_f = 1.58 \mu\text{m}$ and $R_f = 0.14 \mu\text{m}$.

The cell body torque can be calculated from the measured swimming speed

$$T_c = \beta_c \omega_c - \gamma_c v_h \quad (30)$$

For stuck bacteria which rotate but do not translate v_h is zero and simplifies to

$$T_c = \beta_c \omega_c \quad (31)$$

To eliminate the influence of viscosity, all the Resistive Force Theory calculation are presented as T/η .

Chapter 3: Effects of pH on Motility of *H. pylori* in BB10 and PGM

In this Chapter, a manuscript which is under review for Science Advances is reproduced. All the experiments, data acquisition and initial analysis were mostly performed by previous Bansil Lab members Clover Su and Katarzyna Bieniek. Based on the data provided and initial analysis, I further helped analyzing the microrheology, speed distribution and trajectory displacement of *H. pylori* and torques estimation.

Intrinsic swimming dynamics influences motility of H. pylori under acidic conditions and sol-gel rheology of mucin manifests in mechanosensing the gel.

C. Su^{1†‡}, K. Bieniek¹, W. Liao¹, M. A. Constantino^{1,§}, S. M. Decker¹, B. S. Turner^{1,2}, R. Bansil^{1*}

¹ Boston University, Boston MA 02215.

² Massachusetts Institute of Technology, Cambridge MA 02139.

† This work is a part of the Boston University Ph.D. dissertation of C. Su.

‡ Present Address: Mass. General Hospital, Charlestown MA 02129.

§ Present Address: National Cancer Institute, NIH, Bethesda, MD 20892.

Email of Corresponding Author: rb@bu.edu

3.1 Abstract

To colonize on the epithelium the gastric disease-causing bacterium *Helicobacter pylori* has to swim across a gradient of pH from 2-7 in the mucus layer. Previous studies have shown that at pH below 4 *H. pylori* do not swim in porcine gastric mucin (PGM) gels. To separately assess the influence of gelation of PGM and that of pH on motors and pH sensitive receptors of *H. pylori*, we used phase contrast microscopy to compare the translational and rotational motion of *H. pylori* in PGM *versus* Brucella broth (BB10) at different pHs. We observed that decreasing pH leads to decreased fraction of motile trajectories and decreases the contribution of fast swimmers in the distributions of swimming speeds and length of trajectories. At all pH's the bacteria swim faster and have longer trajectory lengths in BB10 as compared to PGM. While bacteria are stuck in PGM gels at low pH's they swim at low pH in broth, *albeit* with reduced speed. The body rotation rate and estimated cell body torque are weakly dependent on pH in BB10, whereas in PGM the bacteria stuck in the low pH gel rotate faster than the motile bacteria and the torque exhibits a peak around pH 4. Our results show that *H. pylori* has optimal swimming under slightly acidic conditions and exhibits mechanosensing when stuck in low pH mucin gels.

3.2 Introduction

The human stomach presents one of the harshest environments due to the high acidity of its gastric juice secretion and various aspartate proteases and digestive enzymes which are crucial for metabolizing food and destroying microbes. To prevent the stomach from being digested by its own acidic secretion and control the transport of food, microbes and

other ingested products, the epithelial surface of the stomach is lined with a protective, continuous, viscoelastic layer of mucus varying from 100-400 μm in thickness. Across this mucus layer there exists a pH gradient maintained by the co-secretion of bicarbonate^{40,41,42} with almost neutral pH close to the epithelial surface and highly acidic pH 2- 4 on the luminal side during active acid secretion. The pH of the stomach measured at the luminal surface has been shown to range between 0.3 and 2.9^{43,44} with the resting median pH close to 1.74⁴⁴ while the resting pH measured in the mucus layer has been shown to be close to 4⁴³. The mucus derives its viscoelastic properties from the glycoprotein mucin which has been shown to undergo a pH dependent sol to gel transition at pH 4^{45,46} forming an elastic gel below pH 4. Exactly how the gelled mucin prevents the back diffusion of H⁺ ions is a subject of considerable debate and various processes such as Donnan equilibrium, diffusion, viscous fingering has been invoked.

While the combination of gastric juice and the gastric mucus is quite effective in sterilizing and protecting the host from bacteria and infections, the gastrointestinal pathogen, *Helicobacter pylori* is known to breach this barrier and has adapted to this particularly challenging environment and colonized human stomachs, perhaps since the beginning of the human species⁴⁷. *H. pylori* colonizes on the epithelial surface and even deep in the gastric glands, leading to the development of diseases such as gastric ulcers, gastritis, and even cancer. The role of stomach pH is one of the most important factors in controlling the colonization and pathogenic effects of *H. pylori* and many questions still remain poorly understood. Using their flagella-driven motility and further aided by chemotaxis mechanisms *H. pylori* navigates towards the neutral epithelial surface where

it attaches using various adhesins and evokes an immune response and can cause inflammation of the surrounding tissue. Moreover, it is well known that *H. pylori* has anti-pH tactic chemoreceptor proteins that are sensitive to the environmental pH change, in particular, *TlpB* protein that are found in the inner membrane of *H. pylori* help it to move away from acidic pH¹⁰. In order to do so, the membrane-spanning *TlpB* proteins are activated by the protons in the environment, which triggers response of a cascade of chemotaxis proteins, such as CheY, CheW, and CheA¹⁰. The net response from the chemotaxis proteins contributes to the rotation direction and rate of the flagella motor, influencing the rate of reversal, persistence of track direction and speed of the bacteria. Furthermore, mucin itself a chemoattractant, is known to gel below pH 4 impeding the motility of the bacterium. Unraveling the intertwined effect of pH on the bacterium and the medium through which it swims is clearly of importance to addressing how *H. pylori* breaches the pH and protective mucus barrier and to the development of strategies to control the very first step of infection. Moreover, it presents an interesting case for the hydrodynamics of swimmers involving the coupling of pH effect on motors and pH sensing receptors along with a pH dependent change in the rheology of the medium transitioning from a sol to a gel. To the best of our knowledge the decoupling of these factors has not been addressed before.

Our group has previously reported that *H. pylori* shows no translational motion in porcine gastric mucin (PGM) solutions below pH 4 in the absence of urea, although rotation of their flagella could be observed in bacteria trapped in the mucin gel network^{5,48}. As reported in these previous studies upon adding urea the bacteria were observed to

simultaneously raise the pH of the surrounding medium and swim as the mucin gel transitioned to a solution. However, it is not clear from this previous study how much of the observed pH dependent change in motility is due to the gelation of PGM and how much is due to the influence of pH on the flagellar motors, as the motors are driven by the transmembrane gradient of protons (H^+), i.e. the proton motive force, PMF⁴⁹. The proton motive force (PMF) is related to the sum of the differences in pH, ΔpH , and membrane potential gradient $\Delta\Psi$ across the inner membrane separating the cytoplasm from the periplasm ($PMF = -61\Delta pH + \Delta\Psi$). While the cytoplasmic pH of *H. pylori* is regulated due to urease activity and remains between 6-7 for external pH between 5 and 8, the periplasmic pH is close to the external medium pH, as shown by direct measurements of both cytoplasmic and periplasmic pH using fluorescent dyes⁵⁰. Sachs *et al.* measured the transmembrane potential for *H. pylori*, $\Delta\Psi = PMF + 61\Delta pH$ ¹⁸ finding a monotonic change in $\Delta\Psi$ from -175 mV at pH 7.5 to -25 mV at pH 4 and becoming close to zero at pH 3.5. These data are consistent with the observation that in the absence of urea *H. pylori* survives between a pH of 4.0 and 8.0 *in vitro*, and does not grow at a pH less than 5.0, i.e. it behaves as a neutrophile in standard buffers, not surviving extreme acidity or alkalinity.

Previous studies on *E. coli* and *Salmonella* revealed that motility is not affected by external pH but by the internal, i.e. cytoplasmic pH of the cell. Internal pH can be modified by addition of a weak acid in the medium because weak acids are known to permeate biological membranes. For example, in *E. coli* and *Salmonella* in the presence

of a weak acid decreasing pH leads to decreasing swimming speeds⁵¹, enhancement of tumbling⁵², and reduced motor rotation rates⁵³. In contrast, *B. subtilis* shows a decrease in swimming speed but a reduction in tumbling⁵⁴ in a low pH environment. *H. pylori* differs from *E. coli* and *B. subtilis* in many ways, for one it is a polytrichous, unipolar bacterium while the other two are peritrichous. Secondly the flagella in *H. pylori* are covered with a membrane sheath. *H. pylori*'s motor has evolved to adapt to a highly viscous and somewhat acidic environment and is capable of high torque generation having 18 stators per motor^{56,57} as opposed to 11 in *E. coli* and 8-11 in *B. subtilis*. The large variation in number of flagella between strains and within bacteria in a given sample further contributes to torque variation. In mucin solutions there will be other factors involved as mucin is both a chemoattractant to *H. pylori* which has specific adhesins that bind to mucin, and its rheology directly influences the hydrodynamics of swimming.

In this work our focus is to separately assess the influence of pH on loss of motility at low pH due to the viscoelasticity of the mucin gel and the influence of increased H⁺ concentration on the flagellar motors and pH sensing chemoreceptors of *H. pylori*. For this we compare the motility of *H. pylori* at different pHs in aqueous brucella broth (BB10) vs PGM. While we have previously investigated motility and rheology at pH 4 and 6^{8,48} and there are some studies of the microrheology of PGM at neutral pH and pH 4^{58,59}, there is no systematic study examining translational and rotational motion of *H. pylori* and the viscoelastic properties of mucin across the entire range of relevant pH's. As expected, we observed that particle motion in broth is purely diffusive, in agreement with the bulk rheology studies reported previously⁴⁷, while that in PGM exhibits a strong

pH-dependent sub-diffusion correlated with increasing heterogeneity at low pH. Our study shows that *H. pylori* swim faster in BB10 than PGM at all pH's, and that motility is hindered at low pH in broth as well as in PGM. In BB10 they swim the fastest at pH 5 indicating that *H. pylori* has adapted its motors for swimming in an acidic environment. In PGM at pH's below 4 bacteria are immobilized due to the gelation of PGM around pH4, although they can still swim in BB10 at these low pHs. From the motion of individual bacteria at high magnification we observed that the body rotation speed is higher when they are immobilized in PGM at low pH as compared to the bacteria swimming at neutral pH, implying that perhaps bacteria are capable of sensing or coupling to the medium's mechanical properties and rotate faster in the gel network. We also estimate torque at different pHs for each of the bacteria imaged at high magnification of 100X using Resistance Force Theory (RFT) following the methods of Magariyama *et al.*⁶⁰

3.3 Results

3.3.1 Microrheology of BB10 and PGM

To measure the microrheology of BB10 and PGM at various pH, we tracked several hundred to thousand trajectories from the Brownian motion of micron-size polystyrene latex particles suspended in the solutions using time-resolved fluorescence microscopy. The mean square displacement (MSD) versus time for each particle trajectory in BB10 and PGM at all pHs along with average $\langle \text{MSD} \rangle$ and relative error are shown in Supplementary Materials, Fig. S1. The viscosity, η , of each solution was computed as detailed in Su *et al.*⁶¹ using the time dependence of MSD for 2-dimensional diffusive

motion of the particles,

$$MSD(t) = 4D_o t \quad (32)$$

where D_o is the diffusion constant. The viscosity is inversely proportional to D_o via the Stokes-Einstein relation,

$$\eta = \frac{kT}{6\pi r D_o} \quad (33)$$

k is the Boltzmann constant, T is the temperature in Kelvin, and r is the radius of the particle. Figure 3.1A shows the $\langle MSD \rangle$ averaged over all particles in BB10 and PGM at various pH on a log-log plot, with water as reference. We found that the $\langle MSD \rangle$ and the viscosity of BB10 are similar to those of water, and not pH-dependent (Fig. 3.3.1A, C).

In contrast, decreasing pH to below pH 4 in PGM leads to significant changes in $\langle MSD \rangle$. It is evident from the log-log plot of $\langle MSD \rangle$ that equation 1 is no longer valid and instead MSD is proportional to t^α . Here the exponent $\alpha < 1$, indicating that the mobility of the micro-particles embedded in PGM is sub-diffusive, i.e. hindered at low pH as a result of the sol-gel transition that PGM undergoes as pH decreases below 4^{7,8}.

The exponent α varies with time reflecting the frequency dependent moduli of the viscoelastic PGM which are presented in⁵⁸. To further describe the sub-diffusive motion of particles in mucin gel at lower pH, we computed the exponent α by fitting the $\langle MSD \rangle$. As pH decreased from 6.7 to 3.7 in PGM, α decreased from 0.8 to 0.6, implying increasing sub-diffusivity of particles in PGM as it gels (Fig. 3.3.1B). In comparison to PGM, the microparticles in BB10 showed normal diffusion with $\alpha = 1$ (Fig. 3.3.1B). Fig. 3.3.1C shows the viscosities of BB10 and 15mg/ml PGM calculated using Eqn. (2). In

the case of PGM the effective viscosity was estimated by using only the data in the short time regime where $\alpha \sim 1$. PGM is about 50 times more viscous than BB10 at pH 6, and the viscosity of PGM increased rapidly, by a factor of 2, as pH decreases from pH 6.1 to 3.7, whereas the viscosity of BB10 remains constant as pH decreases (Fig. 3.3.1C). For the microrheology data in PGM a calculation of the complex viscoelastic moduli was also done as described in Constantino Ph.D. dissertation²¹. The viscosity estimated from the viscoelastic moduli agreed with that obtained from the MSD within 10%. Our results agree with the pH dependent trends observed in bulk rheology measurements using falling ball Martinez viscometry on 10 mg/ml PGM⁶² showing a dramatic increase in viscosity as pH decreases. The viscosity of 10 mg/ml PGM at pH 4 is roughly 15 cP, as pH decreases from pH 4 to 2, the viscosity increases by a factor of 20⁶². At low pH in PGM the elastic modulus approaches and becomes greater than the viscous modulus at low frequencies indicating gelation, although the moduli obtained from microrheology^{49,59,61,58} are lower than those obtained from oscillatory shear bulk rheology^{8,58} or falling ball microviscometry⁶² showing that particles smaller than mesh size do not experience the bulk viscoelasticity. The micro- vs. bulk methods also differ in time scales and shear rates probed. We also note that variation in viscosity values reported by different researchers is mostly due to differences in mucin purification processes, mucin composition and concentration and the sources from which the mucin was collected. However, one can clearly conclude that the overall viscosity increases with increasing mucin concentration and decreasing pH. In the interest of our aim to examine the influence of pH and viscoelasticity on the bacterial motility, we note that is important to

obtain measurements of viscosity and motility from the same set of bacteria in the same batch of purified PGM to provide the most reliable comparison.

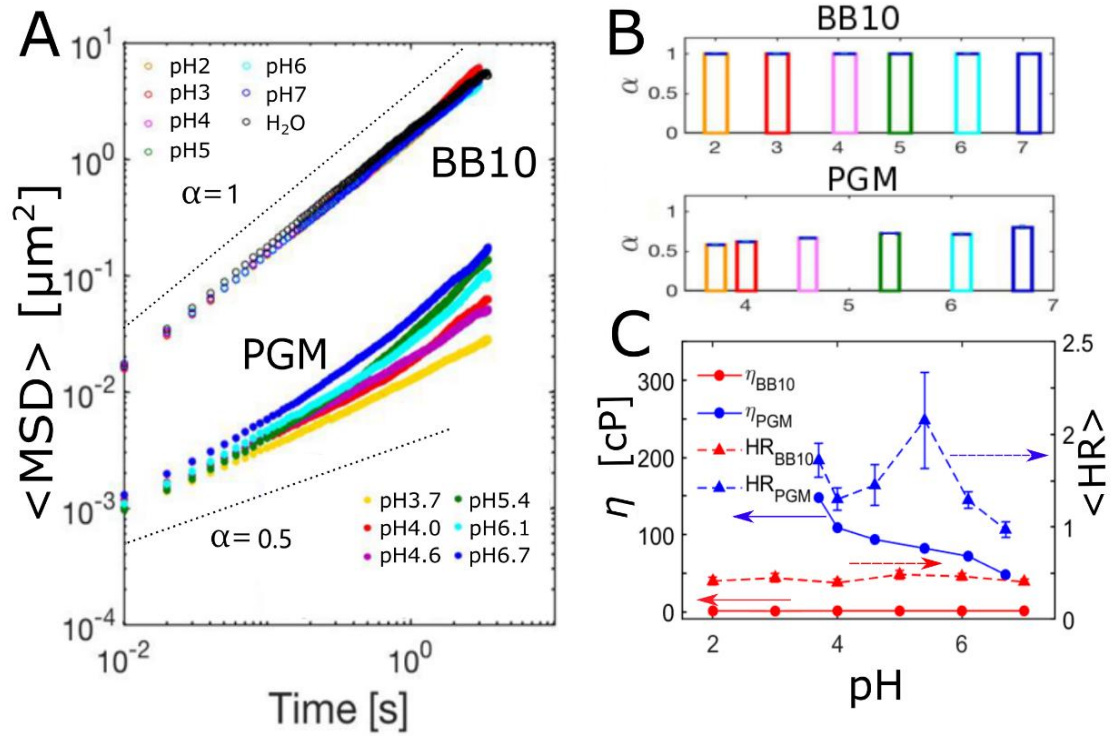


Figure 3.1 Microrheology of BB10 and PGM at various pHs. **(A)** Average mean-square displacement ($\langle MSD \rangle$) of BB10 (hollow symbols), PGM (filled symbols) at pH 2 - 7 averaged across all particles. **(B)** Bar graphs of the exponent α versus pH calculated from $\langle MSD \rangle$ of all particles. **(C)** HR and viscosity η of BB10 and 15 mg/ml PGM calculated as discussed in the text. The arrows in **(C)** point towards the respective axes. The microrheology data for PGM is reproduced from ref ⁶¹ with permission of author.

We evaluate the effect of gelation on mucin by computing the lag-time-dependent spatial heterogeneity (HR) of PGM at various pH following the methods described by Rich *et al.*

⁶³. Briefly, HR is a dimensionless measure of the spatial heterogeneity in a non-homogeneous system, defined by the ensemble variance and the mean of MSD ,

$$HR(\Delta\tau) = \frac{\text{var}(MSD(\Delta\tau))}{\langle MSD(\Delta\tau) \rangle^2} \quad (14)$$

Here $\Delta\tau$ is the characteristic lag time. In particle tracking measurements due to particles constantly diffusing in and out of the focal plane, the ensemble averaging of MSD across all particles in a medium with spatially heterogeneous rheology tends to result in a statistical bias toward more motile particles, as they have higher probability of leaving and re-entering the field of view, producing segmented, shorter tracks. By calculating HR , each trajectory is weighted by a factor proportional to its duration in time. Fig. 3.3.1 C shows the time averaged $\langle HR \rangle$ along with its standard deviation as a function of pH in BB10 and PGM. As a reference from a theoretical calculation, in a bimodal system consisting of 50% water and 50% Newtonian fluid with viscosity ten times greater than water, $HR \sim 0.6^{63}$. At a characteristic lag time of $\Delta\tau = 0.1\text{s}$, we found that $HR_{BB10} \sim 0.1$ at all pHs measured, consistent with BB10 behaving like a watery Newtonian fluid, whereas at $\Delta\tau = 0.1\text{s}$ HR_{PGM} increases from ~ 0.5 to nearly 1 as pH decreased from 6.7 to 3.7 indicative of increasing heterogeneity as pH decreases. The HR data in PGM shows a peak at pH 5, we suspect that this reflects a biphasic behavior of HR , with two characteristics corresponding to the gel phase around pH 4 and lower and the solution phase at pH 5 and above. From AFM measurements⁵⁰ we have shown that PGM fibers which are uniformly distributed at pH 6 begin to show aggregation at pH 5 and this might lead to an increase in $\langle HR \rangle$ as fibers get closer together increasing the available void space in which particles can move. In the gel phase, the particles are excluded from the regions with large concentration of fiber bundles and exhibit hindered motion in the pores of the gel. In this case the inhomogeneity will depend on the extent of crosslinking and

degree of gel swelling/shrinking and this could explain the slight increase from pH 4 to 3, as fibers form tighter bundles due to increased crosslinking at pH 3 relative to 4.

3.3.2 Confocal Imaging of PGM Reveals a Heterogeneous Structure at Low pH

Mucin gels have a hierarchical self-assembled structure at different length scales. While AFM probe the structure of the mucin polymers on scales to a few microns⁷², larger scale structure can be seen by optical microscopy. The phase contrast images of mucin at 100x show fibers in 2 dimensions. To observe the 3-dimensional (3D) structure we obtained DIC confocal images of PGM at pH 3 and pH 6. Movies which show the 3 D structure to better illustrate the aggregation of fibers are included Su dissertation³² and Figure S2 shows a single frame from the movie to illustrate a 2-dimensional cross-section. At pH 6, PGM has a more uniform distribution of mucin strands throughout the field of view. This is also consistent with the more or less uniform occurrence of peaks in the intensity profile taken along a line. In contrast, at pH 3, the intensity profile shows large gaps between peaks, indicating that the gelation of PGM leads to aggregation of mucin fibers giving a non-uniform fiber density, with bundles of fibers separated from regions depleted in mucin fibers. The fiber lengths also appear to vary more in the pH 3 sample, indicative of increased aggregation and crosslinking at low pH. We note that at this resolution it is not possible to observe crosslinks.,

*3.3.3 pH Dependence of Swimming Speed Distributions of *H. pylori* in BB10 and PGM*

To determine how the pH and the viscoelasticity of the environment influence the motility of *H. pylori*, we tracked bacteria from the *H. pylori* J99 strain swimming in BB10 and 15 mg/ml PGM with pH ranging from 2 to 6.3 using phase contrast

microscopy recording time-lapse images at 40x magnification and 33 fps. We performed a detailed analysis of the movies to obtain the bacteria trajectories at each pH in BB10 and 15mg/ml PGM, following the methods described in Martinez *et al.*¹⁸. Briefly, the PolyParticle Tracker program analyzes each trajectory to determine the instantaneous position as a function of time. Fig. 3.3.2 shows images of all recorded trajectories from entire movies at different pHs in BB10 (Fig. 3.3.2A) and in PGM (Fig. 3.3.2B).

We note that the color coding of trajectories is not identified with the time (or the frame number in movies) where the trajectory began, although trajectories which cross each other were clearly from bacteria moving at different times. Different trajectories could arise from the same bacterium going in and out of the image plane; however, the program cannot keep track of which bacterium gave which trajectory. We address this point in the last section by doing single bacteria tracking at high magnification. In the images of Fig. 3.3.2 we are displaying only the trajectories from swimming bacteria, those that were not motile were separately counted. From these images some differences between BB10 and PGM are clearly obvious. First comparing BB10 and PGM, we observe a larger fraction of linear trajectories in BB10 as compared to PGM, in agreement with the finding of Martinez *et al.* that % track linearity is higher in BB10 at pH6 than in PGM. There are fewer trajectories that exhibit a 2-dimensional random walk characteristic in BB10 than in PGM. Trajectories with turns and reversals can also be seen. The trajectories in PGM appear more helical indicating that even at 40X magnification and 33 fps the rotation of the bacterium is visible in PGM but less so in BB10 under these conditions. We further discuss this aspect in the last section using single bacteria imaging at high resolution and

fast frame rate similar to Constantino *et al.*³⁶. Secondly, regarding the effect of pH we note that in both BB10 and PGM there are considerably fewer trajectories at the low pH's as compared to the images at pH > 5 in BB10 and pH > 4 in PGM. We found that in BB10 the bacteria swam over the entire pH range investigated, pH 3 - 6.3, with a decline in the percentage of motile trajectories with decreasing pH, although some bacteria became immotile and coccoidal at pH 3. In contrast to this, in PGM the bacteria swam *only* at pH 4 and higher; there were very few swimmers (~5 in total) in the pH 3.5 sample, and this data was not analyzed, while at pH 3 there were no swimmers; bacteria were stuck and observed to rotate in place at pH 3.5 and pH 3. The percent of motile bacteria was counted by looking at randomly selected frames in the movies. By this method we estimate that in BB10 there are about 40% motile bacteria at pH 3 and 4 and around 60% at pH 5 - 6, whereas in PGM there were only 12% motile bacteria at pH 4, and around 20-25% motile bacteria at pH 4.5, 5 and 6. The reference bacteria from the sample in BB10 were also examined at the same time as the PGM measurements were being conducted and these remained motile confirming that bacteria were viable and that the immotility was due to gelation of PGM not due to loss of motility in the sample.

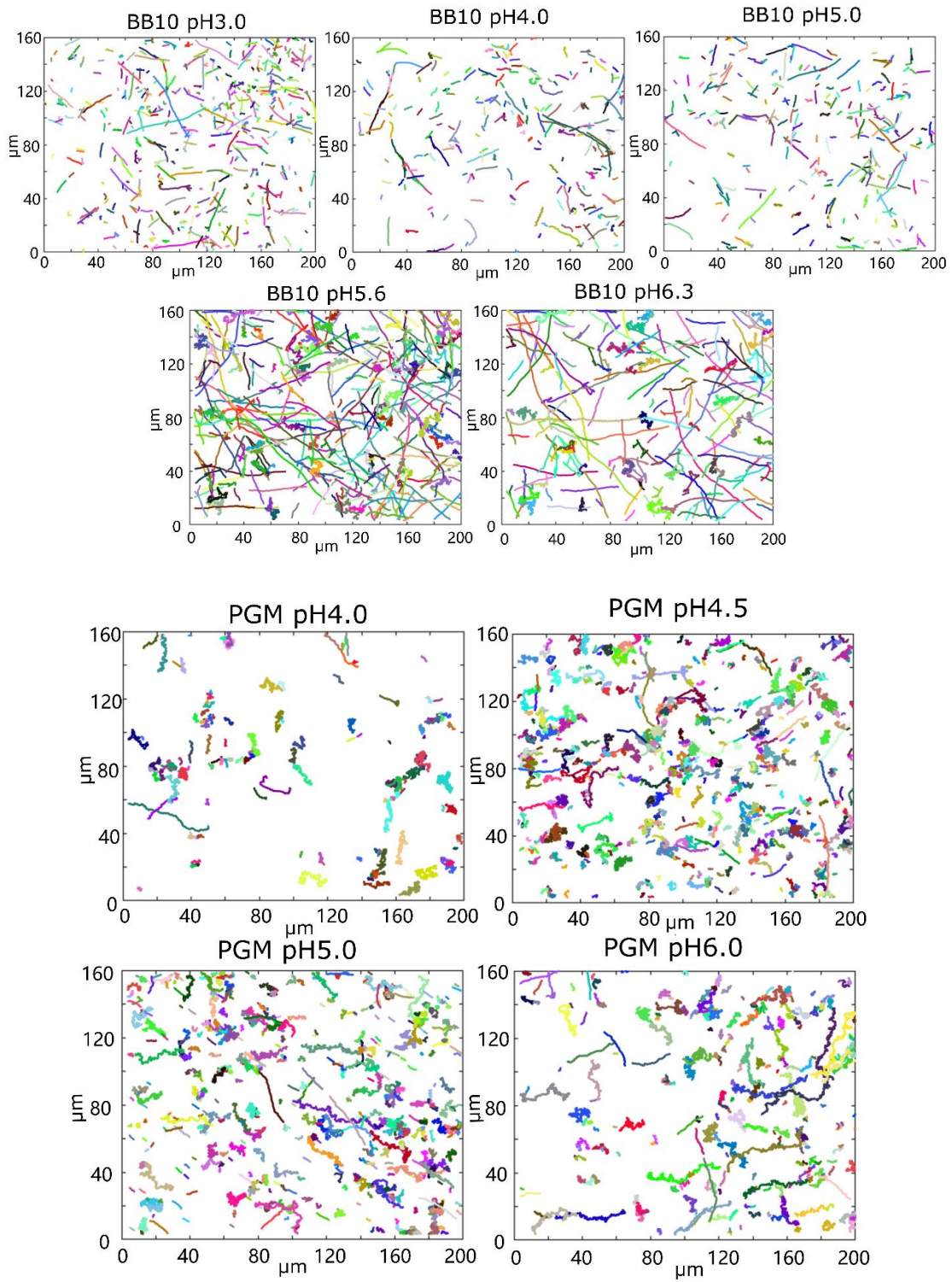


Figure 3.2 Images of trajectories in BB10 (A) and PGM (B) at different pHs as indicated.

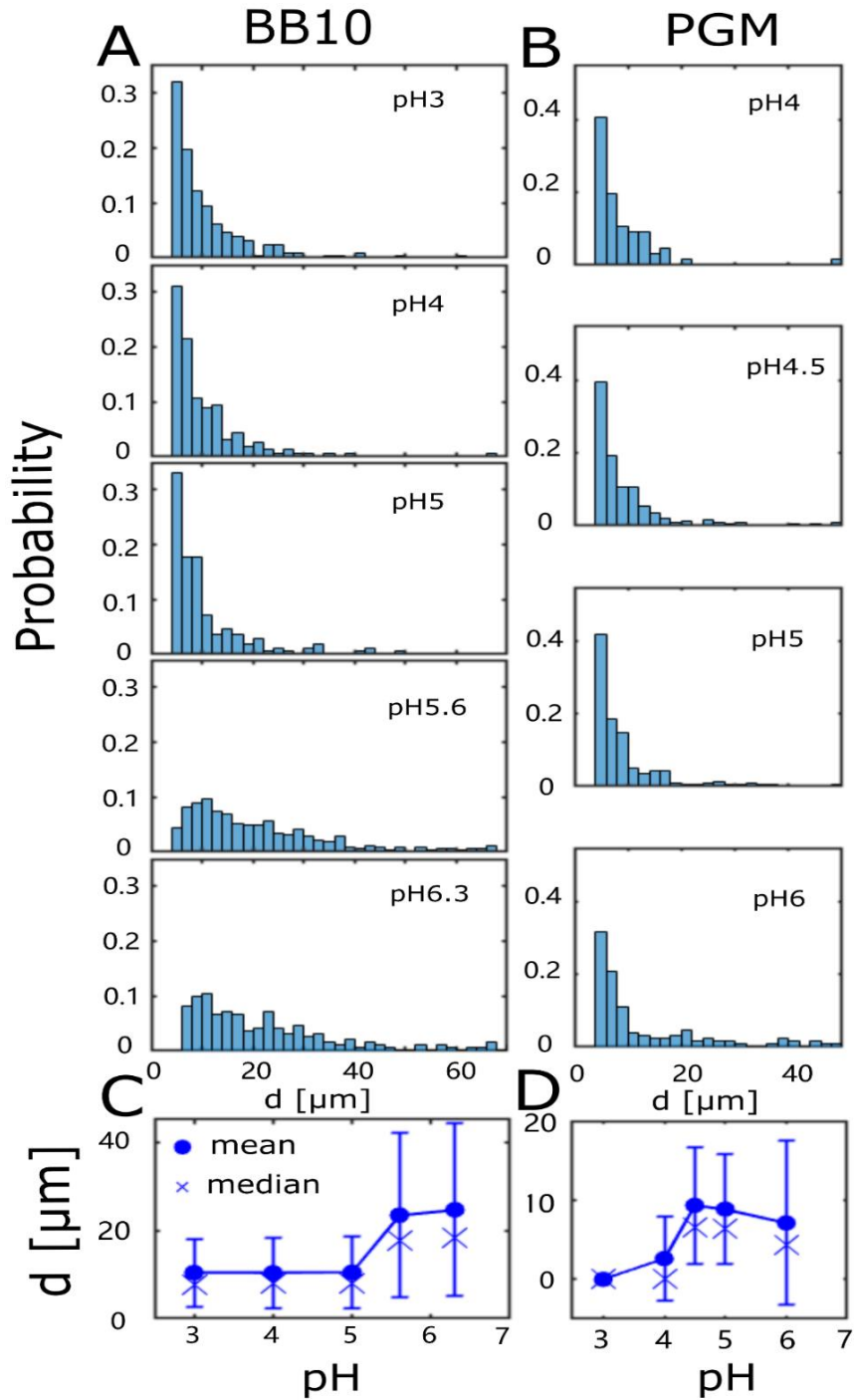


Figure 3. 3 The distribution of trajectory displacements in BB10 (A) and PGM (B) at different pH's as indicated, and the dependence of the average displacement (mean and median) with pH in BB10 (C) and PGM (D). Note that trajectories with $d < 4$ μm are not displayed as these correspond to bacteria which are immotile and only display passive Brownian motion.

From the trajectory we obtain the displacement (d) between the first and last frame, as well as the maximum displacement (d_{max}). For linear trajectories these two measures are the same whereas for trajectories which look like directed random walks d can be less than d_{max} . Fig. 3.4 shows the histogram of the distribution of d for both BB10 and PGM at all pHs. The distribution of displacements extends to larger values for BB10 than PGM and this is reflected in the average $\langle d \rangle$ being about a factor of two larger in BB10 as compared to PGM. In both media, decreasing pH diminishes the occurrence of larger d values and this is reflected in $\langle d \rangle$ dropping by about a factor of 0.4 in BB10 between pH 6 and 5, and a more pronounced drop by a factor of 0.7 between pH 4.5 and 4 in PGM where no motile trajectories are found at pH 3. We attribute these differences between BB10 and PGM to the gelation of PGM around pH 4.

The trajectories were further analyzed by determining the instantaneous speed (v_{ins}), defined as the displacement per unit time between two consecutive time frames, and the direction in which the bacterium was traveling by the change in angle of the displacement vector. *Reorientation events* were identified when bacteria changed the direction in which they were traveling, and when the reorientation angle (θ_{re}) exceeds 140° we considered it as a *reversal*. The reversal frequency defined as the number of reversal events in a trajectory divided by the time duration of a trajectory and % reversals defined as the number of angle changes larger than 140° relative to the total number of all angle changes in a trajectory were calculated. The run speed (v_{run}), is defined as the average speed over a linear path between two reorientations or reversal events. The distribution of both v_{ins} and v_{run} was obtained from the analysis of large number of trajectories, typically

greater than 50, and in many cases up to 200 trajectories were analyzed. The average mean, median and standard deviation (σ) of v_{ins} and v_{run} , as well as the percentage of motile trajectories were determined at each pH in BB10 and PGM. As discussed in our earlier work, the standard deviation σ is a measure of the width of the distribution and reflects both the temporal variation in speed, as well as the variation in speed largely due to the polydispersity in number of flagella as well as in helical shape and size of the bacteria in a given sample⁵³.

Figure 4 shows the histograms of distributions of v_{ins} and v_{run} in BB10 (**A**) and PGM (**B**) at different pHs. Both the speed distributions are broad and appear to be clearly bimodal in BB10, with a peak from slow swimmers in the vicinity of 10-15 $\mu\text{m/s}$ and that of fast swimmers around 40-50 $\mu\text{m/s}$. In BB10 (Figure 4 **A**) we can clearly see two peaks in v_{ins} distribution, and a high-speed tail in distribution of v_{run} at pH 5.6 and 6.3. At lower pHs the peak corresponding to the faster swimming shifts from around 50 $\mu\text{m/s}$ at pH above 5 to around 40 $\mu\text{m/s}$ at pH 5 and lower. At pH 5 the speed distributions in BB10 are very broad because the slow and fast peaks overlap, although two peaks are still visible in the distributions. At pH 5.6 and 6.3 there are several bacteria swimming at very high speeds ($> 60 \mu\text{m/s}$). The speed distribution for the slower bacteria (speed $< 25 \mu\text{m/s}$) appear to be less influenced by pH. In PGM the speeds are lower than in BB10 at all pHs and there are very few swimmers with speeds exceeding 30 $\mu\text{m/s}$ in PGM (the probability is small so they cannot be identified in the histogram). However, the distribution of speeds displays an asymmetric profile at the higher speeds, indicating that bimodality of speeds is present, although to a much smaller extent than in BB10. We have fit this data to two

peaks and the results presented in Supplementary Materials Fig. S3 agree with the statements made above by visual inspection of the speed distribution histograms. We also calculated the mean instantaneous and run speeds, $\langle v_{ins} \rangle$ and $\langle v_{run} \rangle$ as well as the median speeds and the standard deviation σ for the entire distribution as shown in (Fig. 3.4 C) for BB10 and PGM (Fig. 3.4D), respectively. Variation in the overall average is influenced by the 2 peaks character of the distributions. In BB10 the average speeds of these broad distributions appear slightly dependent on pH, whereas in PGM the speed goes to zero at pH 3, but otherwise is hardly influenced by pH in the solution phase. As discussed later, in considering the effect of pH in PGM we have to consider the highly negatively charged polyelectrolytic property of mucin which influences the ratio of bound vs free H⁺. The distribution of turn angles, θ_{re} at different pHs is shown in (Fig. 3.4 E, F) for BB10 and PGM, respectively. It clearly shows that there are fewer reversals in PGM at all pHs as compared to BB10, with a cumulative probability of turns between 150°–180° ranging around 0.25 in BB10 and less than 0.1 in PGM. In PGM there were more reversals at pH 4 as compared to the higher pHs presumably reflecting the effect of gelation at low pH in PGM (Fig. 3.4F). The reversal frequency obtained by ensemble averaging of the number of reversals divided by the time duration of each trajectory varies from 10 to 2. More than half of the turn angles in BB10 are below 90° whereas in PGM this fraction is higher approaching around 80% (cumulative probability is 50% to 67% in BB10 and 78% to 94% in PGM).

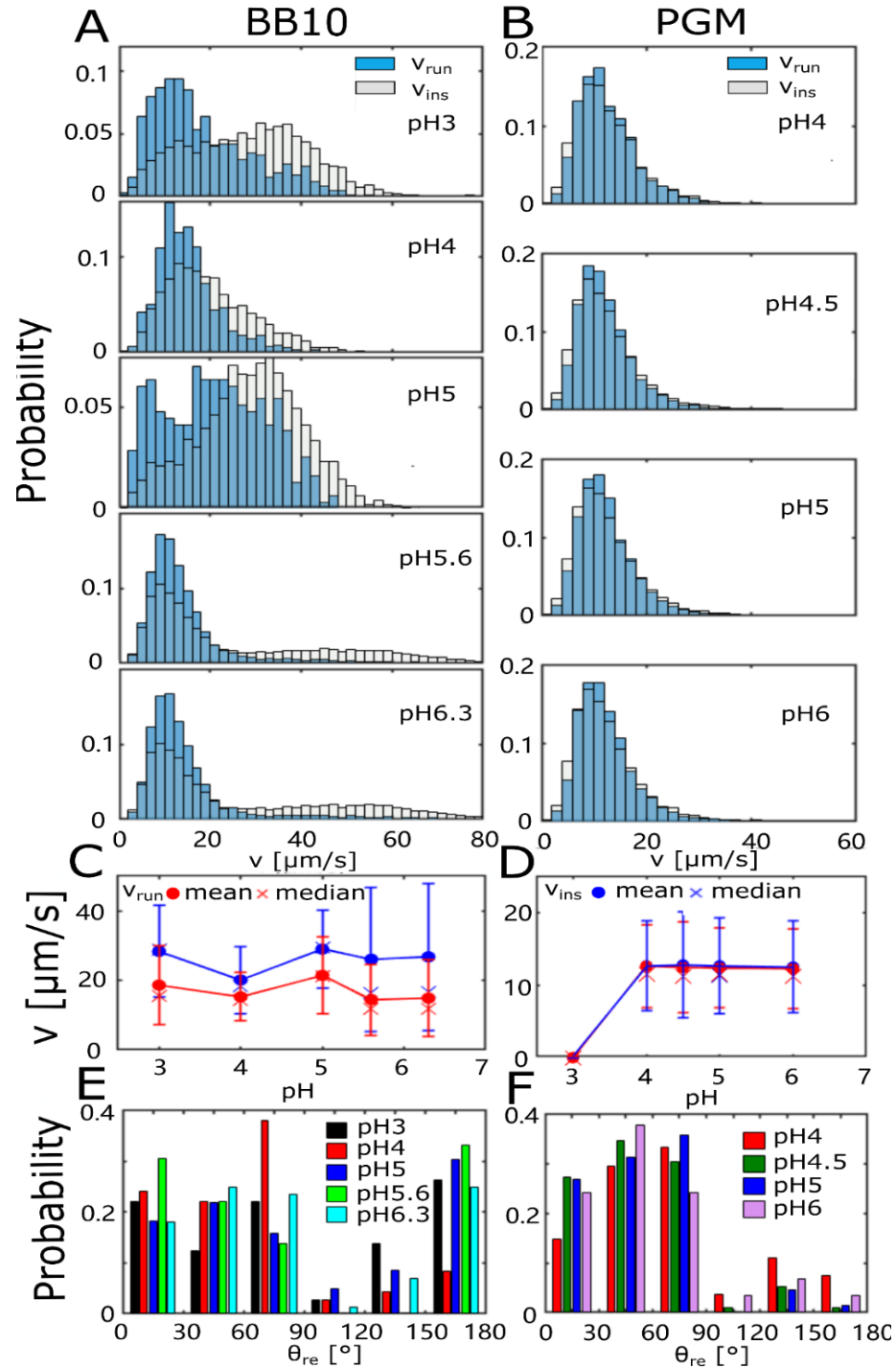


Figure 3. 4 Distributions of swimming speeds and turn angles of *H. pylori* J99 strain in BB10 and PGM at various pH. Histograms summarizing the instantaneous speed (v_{ins}) (no color) and the run speed (v_{run}) distributions (blue) in BB10 (**A**) and PGM (**B**) are shown at different pHs as indicated. When the two histograms overlap the outline of the v_{ins} histogram is visible over the blue histogram.

3.3.4 The Effect of pH on Cell Body Rotation in BB10 and PGM.

While there have been some previous results about effect of pH on swimming speeds, to the best of our knowledge there is no previous study about the effect of pH on *H. pylori*'s rotation. To measure the effect of pH on cell body rotation we imaged the motion of bacteria at a high magnification 100X and fast frame rate 100-200 fps as was previously done for *H. pylori* at neutral pH by Constantino *et al.*³⁶. Each frame from the trajectory of a single bacterium recorded as the bacterium rotates and translates was analyzed using the CellTool program²⁹ to obtain the cell body rotation.

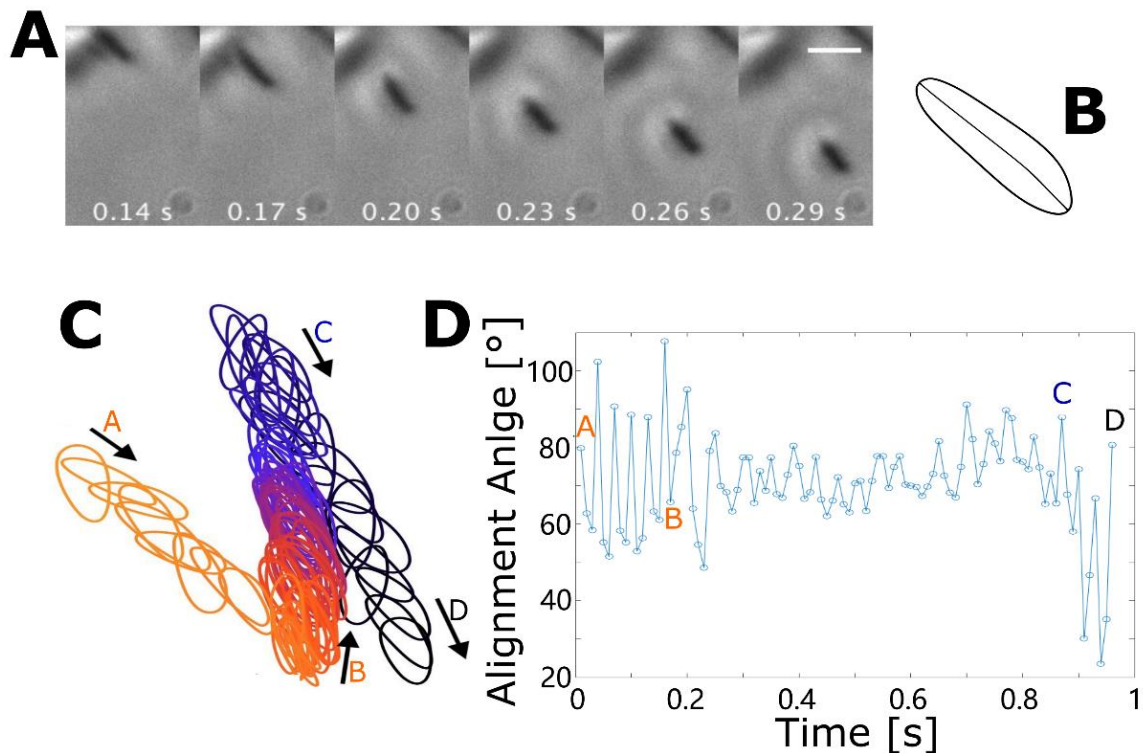


Figure 3.5 A, B, C, D Rotation of cell body as the bacterium swims. **(A)** A series of frames showing the image of a single bacterium at 100X as it rotates while translating in BB10 at pH 4. **(B)** A typical contour and the center line obtained from CellTool. **(C)** Successive contours along the bacterium's trajectory. The points A, B, C, D indicate reorientation events as described in the text. The frames shown in **(A)** are from the motion segment, A to B. **(D)** Alignment angle (with reference to an arbitrary direction) showing oscillations as the cell rotates. The movie for this data are obtained from Su dissertation³².

A few frames from one bacterium shown in Fig. 3.5A clearly show that the bacterium is rotating about an axis related to its flagella axis as it swims. As discussed in Constantino *et al.*³⁶ the axis of the flagella and that of the cell body are not colinear, in other words the motion is like a precession. A typical contour and alignment axis of the bacterium obtained by CellTool is shown in Fig. 3.5B. This analysis was done for each frame of all the bacteria that could be imaged at different pHs in BB10 and in PGM.

Figure 3. 5C shows successive contours along the trajectory of the bacterium of Fig. 3. 5A which shows the bacterium swimming forward as a pusher (A to B in the figure), then reversing to swim backwards (B to C) and reversing again at C to swim in the forward direction to the point D.

The spacing of successive contours indicates that the bacterium is moving slower while it is in the reverse mode. In the movie (Su dissertation³²) we can see flagella sometimes which enables us to identify the pusher or puller (forward or reverse) motion. Figure 3. 5D of alignment angle as a function of time shows clear oscillations as well as the larger reorientations as trajectory changes direction between runs. From these data we can obtain the speed and frequency over each oscillation as well as the average speed V over the entire trajectory and the average rotation rate Ω . Because the images of cells are sufficiently clear at high magnification, when the bacterium image is fully in the image plane we can get good estimates of its length, thickness and helical pitch, and number of turns in the helix. We note that the speed measurement at this high magnification is from shorter trajectories than the ones reported in Fig. 3.3.2 from 40X imaging because the depth of focus is smaller and bacteria remain in focus for only short times. Moreover,

some fast bacteria move out of focus so rapidly that they cannot be recorded. Due to these experimental limitations only a few bacteria could be tracked at high magnification and thus the swimming speed observed may not be statistically representative of the whole population of bacteria. In view of these limitations we focus on the body rotation rate from these high magnification measurements, which is quite constant over the short runs (see Fig. 3.5D). We also calculated the ratio V/Ω which is a measure of the distance travelled by the bacterium in one rotation. As discussed in the regularized Stokeslet modeling of the bacterium's motion in Constantino *et al.* the ratio V/Ω is independent of the flagella rotation rate³⁶. The flagella rotation rate varies not only temporally but also from one bacterium to another as they have different number of flagella⁵⁸, and thus the ratio V/Ω is also independent of the number of flagella in each bacterium. Figure 3.5(E, F) show the bacteria cell body rotation rate (Ω) at different pHs in BB10 and PGM, respectively. By comparing bacteria in BB10 with those in PGM we note that while the rotation rate spans a similar overall range in PGM and BB10, the ratio V/Ω is about a factor of 5 smaller in PGM as compared to BB10 (Figure 3.5 G, H). This is consistent with the observation that due to the higher viscosity of PGM the bacteria swim slower in PGM than in BB10 (see the 40X measurements of Fig. 3.4). The rotation rates that we observe for J99 in pH 6 in BB10 and PGM are similar to those reported by Constantino *et al.*³⁶ for the LSH100 strain which has similar average number of flagella as J99^{61,28,64}. A comparison of Fig. 3.5E and 5F shows that the rotation rate in BB10 is more or less unchanged by pH varying from pH 6 to 4 and then decreases as pH decreases to 3. The rotation rate in PGM exhibits a more complex behavior as below pH 4 the bacteria do not

translate but still rotate⁴⁸. In the pH range where bacteria can swim in PGM, the rotation rate decreases as pH decreases from 5.5 to 4.5, and then increases reaching a peak value at pH 3.5 and dropping slightly as pH drops to 3. The increase in body rotation frequency below pH 4 in PGM correlates with stuck bacteria suggesting an increased rotation speed of flagellar motors in a mechanosensing response to the increase in viscosity as pH approaches a sol to gel transition on decreasing pH below 4 (see microrheology data in Fig. 3.3.1). The rotation of stuck bacteria has previously been reported by Celli *et al.*⁵, although they were not able to compare rotation rates of stuck *vs* motile bacteria. We find that the values of the stuck bacteria rotation rate that we obtained are over one order of magnitude higher than the ~3–10 Hz reported by Celli *et al.*⁵, which could just have been specific to the single bacterium they imaged, but also reflect the differences due to the different strain of *H. pylori* used in this study as compared to Celli *et al.*⁵ whose measurements were also at a slower frame rate (30 fps) and they only measured a couple of stuck bacteria. The movie reported by Celli *et al.* of the bacterium shows a large temporal variation in both body and flagella rotation rate.

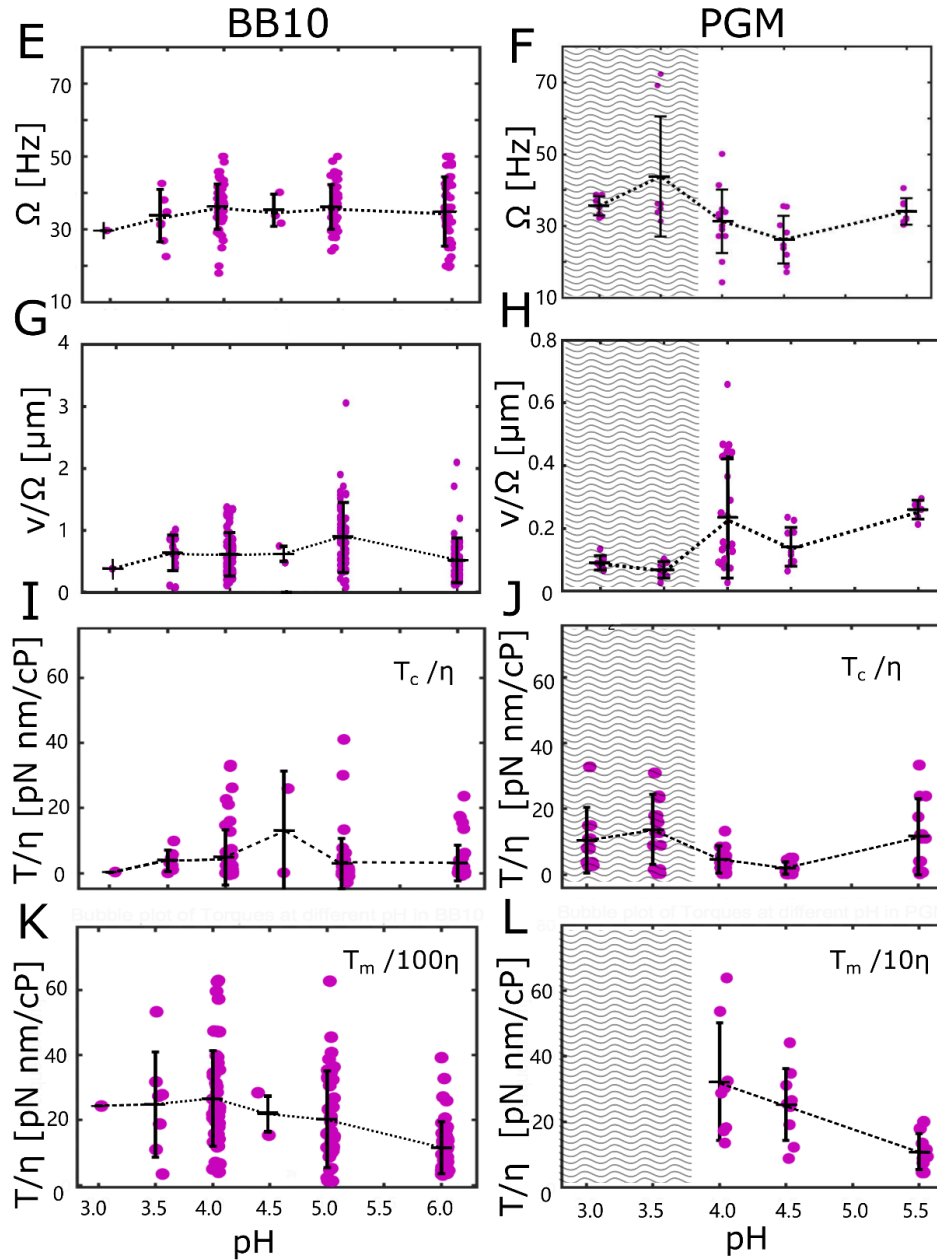


Figure 3.6 E, F, G, H. The bubble plots in **E, F, G, H, I, J** show cell body rotation rate (Ω) of J99 in BB10 (**E**) and PGM (**F**), the ratio V/Ω in BB10 (**G**) and PGM (**H**), estimated cell body torque T_c in BB10 (**I**) and PGM (**J**), and motor torque T_m in BB10 (**K**) and PGM (**L**) calculated as described in the text for all of the bacteria imaged at pH 3 to 6. Note that T_m was not calculated for stuck bacteria for reasons discussed in the text. Cell body torque is plotted as T_c/η and motor T_m is plotted as $T_m/(100\eta)$. The mean and standard deviation are indicated. The dashed lines are a guide to the eye. The gray shaded region represents the pH range over which PGM gels and bacteria did not translate but only rotated.

3.3.5 Estimation of Torque using Resistance Force Theory (RFT)

We estimated the torque for individual bacteria whose rotation rates and swimming speeds are presented in Fig. 3.5 **E - H** using RFT and a helical body as was done in Martinez *et al.*¹⁸ This is an improvement over the previous calculation in Celli *et al.*⁴⁸ which was only done for stuck bacteria assuming an ellipsoidal body shape. The RFT model we used was described in Magariyama *et al.*⁶⁰. Briefly, RFT decouples the flagella and cell body motion and thus forces and torques on an object are proportional to the local speed and angular rotation rate of that object, with the proportionality determined by the viscosity and the object's geometry via hydrodynamic drag coefficients. The flagella and cell body satisfy force – torque balance and this enables calculation of the torques on both cell and flagella and the motor torque. We emphasize that RFT is an estimate and has limitations both due to decoupling and assumptions such as implemented here with the flagella and body axis taken as colinear. More detailed studies could be done using Regularized Stokeslet model (RST)³⁶. An additional caveat is that neither RFT or RST model swimming in viscoelastic media, such as PGM. Using the condition of zero net torque: $T_m - T_f = 0$, the motor torque T_m can be estimated from flagellar torque T_f which can be estimated from bacterial translational speed v_h and shape factor S_h . For swimming bacteria, motor torque T_m was calculated from

$$T_m = v_h/S_h. \quad (35)$$

We used the measured speed for each bacterium imaged at 100X in PGM and BB10 at different pH and the shape factor S_h for a helical body and helical flagellum using the equations of Martinez *et al.*¹⁸ to calculate corresponding torque. (see the Methods

section). The cell shape parameters of each bacterium were measured from the 100X images while the flagella parameters (not measured here) were set the same as in Constantino *et al.*³⁶ The cell body torque T_c can be calculated from the measured swimming speed and cell body rotation rate

$$T_c = \beta_c \omega_c - \gamma_c v_h \quad (36)$$

The hydrodynamic coefficients β_c and γ_c was obtained using the equations of Martinez *et al.*¹⁸ (see the Methods section for expressions for β_c and γ_c). For stuck bacteria which rotate but do not translate v_h is zero and we obtain from Eq. (5),

$$T_c = \beta_c \omega_c \quad (37)$$

The hydrodynamic coefficients are all proportional to the viscosity η and thus torque is proportional to η . While η is close to 1 cP for BB10, which is a Newtonian fluid, the choice of what to use for η for PGM is complicated because mucin is a non-Newtonian shear thinning fluid and at low pHs it is a viscoelastic fluid^{21,46}. Furthermore, our previous studies of particle tracking microrheology of PGM in the presence of active, swimming *H. pylori* bacteria have shown that the probe particles exhibit enhanced diffusion due to the active swimmers^{59,61}. The enhancement reflects the advection of particles as bacteria swim through the fluid as well as the shear thinning that bacteria motion produces in PGM and is more pronounced in the solution state at high pH as compared to the gel state. The advection also occurs in BB10, although it is less pronounced. In our previous work we obtained a factor of 12.6 enhancement in D of latex particles in the presence of J99 bacteria in PGM, implying an effective viscosity 5 cP in for J99 bacteria swimming in PGM at pH 6. In view of these complications we plot

the ratio T_c/η calculated using the equations above in Fig. 3.5 I and J for each of the bacteria imaged at 100X as a function of pH in BB10 and PGM, respectively. The calculation of T_c was done both for the stuck bacteria at low pH and the motile bacteria at higher pH. We find that the average ratio T_c/η in BB10 is comparable to that in PGM, however the actual torque in PGM will be higher scaling in proportion to the viscosity. Using the actual viscosity of purified PGM (see Fig. 3.3.1) we get T_c to be about two orders of magnitude higher in PGM as compared to BB10. A more realistic estimate would be obtained if we used the value of effective viscosity measured from particle tracking in PGM with active J99 *H. pylori* bacteria. In that case we obtain a torque T_c which would be about 10 times higher in PGM than in BB10 at pH 6 and about 20 times higher in PGM at pH 4. Hydrodynamic drag plays a bigger role in the more viscous PGM than in BB10. For motor torque the estimates for BB10 shown in Fig. 3.5K increase from 1000 to 2000 pN. nm over the pH range 6 to 4 and remain more or less constant below that down to pH 3. On the other hand, in PGM using the viscosity of pure PGM from Fig. 3.3.1, motor torque would increase from a rather unrealistic value of 5000 pN. nm at pH 5.5 to 10,000 pN. nm at pH 4, whereas it would increase to more realistic values of 500 pN.nm at pH 5.5 to about 1000 pN.nm at pH 4, taking into account the reduction in effective viscosity of PGM due to shear thinning and convection effects in PGM solution with active swimming bacteria.

In both media the variation among different bacteria imaged at the same pH is larger than the variation of the average with pH. The dependence of cell torque vs pH for PGM may not directly correlate with the peak in Ω because we imaged individual bacteria which

vary in size/shape/ flagella number in the different measurements. Torque is proportional to viscosity and hydrodynamic drag terms dependent on the size and shape of the bacterium. If all measurements were done with the same identical bacterium having identical flagellum then according to RFT torque in broth would be independent of pH and that in PGM would increase with decreasing pH reflecting the increasing viscosity of PGM as pH decreases. However, in our experiment we imaged individual bacteria which vary in size/shape/ flagella number, and the observation of a peak in Ω at pH4 in PGM cannot be simply interpreted as the effect of pH on torque. We used the flagella parameters from our previous Regularized Stokeslet modeling calculations³⁶ and estimated a motor torque about 100 times larger than cell body torque for motile bacteria in BB10 and 10 times larger in PGM (see Figs. 5I and J). For the case of stuck bacteria in PGM we cannot estimate the motor torque without additional assumptions because we could not measure the flagella rotation rate in our experiments. Furthermore, stuck bacteria which rotate but do not translate may have additional torques from the interactions between the bacterium and the medium which hold it in place.

3.3.6 Different Types of Stuck Bacteria

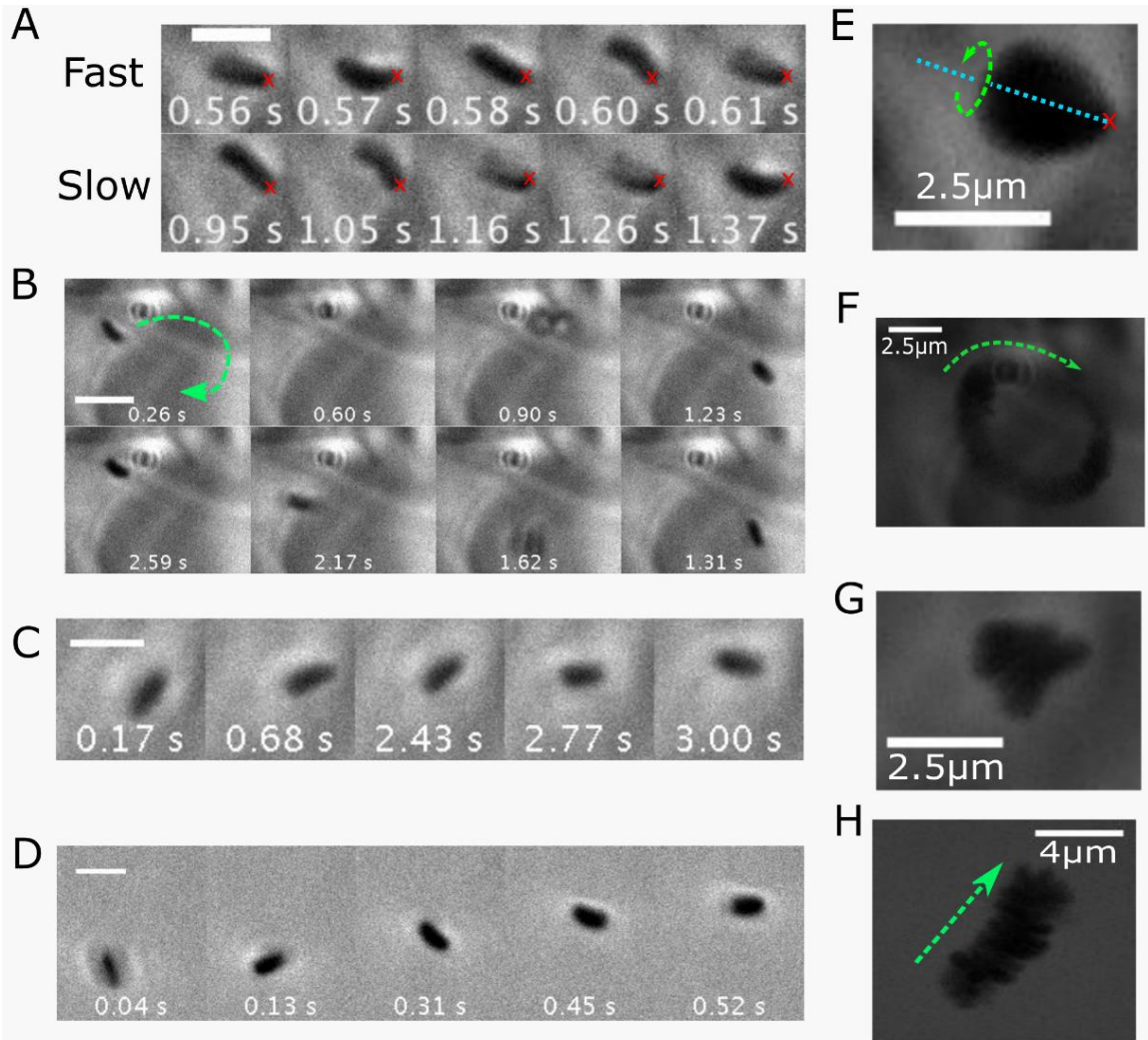


Figure 3. 7 Phase contrast microscopic time-lapse montages and trajectories of various modes of bacteria stuck in PGM at low pH. **(A)** Bacterium appears to rotate about a fixed point (indicated by the red x) with fast and slow body rotation rate over time. **(B)** Bacterium moves in a fixed circular trajectory perhaps reflecting proximity to a region of high PGM concentration (dark region) Time increases going clockwise through the images. **(C)** Bacterium at pH 4.5 in PGM showing rotations along with small, random rotations along with small, random translational displacements. **(D)** Bacterium in BB10 at pH 4 shows a clear translation while rotating. The scale bars in **A-D** indicate a length of 2.5 μm. The images in **E, F, G, H** are overlays of different frames of the movie onto a single image to show the trajectory corresponding to **A, B, C, D** respectively, with the green arrows indicating the direction of motion. The movies for this data are provided in Su dissertation³².

Figure 3.7 shows some images of bacteria stuck in different ways, obtained from the Su dissertation³². Along with a few images at different times as indicated, we also show the trajectory of the bacteria by plotting their positions over the entire movie as a single image (Fig. 3.7 **E-H**). For e.g. one bacterium appears to be stuck at the flagella end (Fig. 3.7 **A**). Fig. 3.7 **B** images show a pair of bacteria with one of them swimming in a small circle, while the other is in a orthogonal position. A bacterium at slightly higher pH 4.5 shows a small amount of translation with a few reorientations while it rotates (Fig. 3.7 **C**). In contrast, the bacterium in BB10 at pH 4 clearly swims in a straight run (Fig. 3.7 **D**). Thus, it appears that bacteria can get stuck by having either their flagella or their body or both get entangled with the polymeric gel-like medium.

3.4 Discussion

We have compared the effects of varying pH and viscosity on the motility and body rotation of *H. pylori* in aqueous broth and PGM solutions. Our results show that the swimming of *H. pylori* in PGM is influenced by the intertwined interactions of pH on flagella motors, pH sensitive receptors and the pH dependent viscoelasticity of mucin while the effect of pH on the motility in BB10 reflects only the effect of pH on the flagellar motor and pH sensitive receptors. We observe that at all pH's where the *H. pylori* bacteria are motile they swim on average with about two times longer trajectories and about two times faster speeds in BB10 as compared to PGM. The swimming speed and trajectory displacement distribution extend to higher values in BB10 as compared to PGM and decreasing pH primarily diminishes the contribution of the longer and faster swimmers. In BB10 bacteria were observed to swim even at the lowest pH measured,

whereas in PGM below pH 4 the bacteria are trapped in the gelled mucin and do not translate but only rotate in place, in agreement with previous reports⁴⁸. Moreover, PGM is a negatively charged polyelectrolyte and it is well known that H⁺ are trapped in the mucin gel due to Donnan equilibrium effects. Titration studies of PGM have shown that the fraction of free protons is reduced with decreasing pH, and in fact the pH of the medium is always higher than that of the external buffer added. As a consequence, the effect of pH on flagella motors for bacteria swimming in PGM will be less than the effect in BB10. All these observations suggest that while in BB10 the flagella motors are impaired at low pH, in PGM the effect of gelation of the medium plays a dominant role. We estimated the torque for the cell body rotation and the motor torque in the case of motile bacteria using RFT to decouple the motion of the helical body from the helical flagella. The torque also shows a peak in PGM following similar non-monotonic trends as observed for speed and rotation rate. The magnitudes of the torque we obtained for *H. pylori* are higher than for other bacteria like *B. subtilis* and *E. coli*, presumably due to the larger number of stators (18 vs. 11)^{56,57} and differences in the bundling of multiple unipolar vs peritrichous flagella. The faster swimmers are more likely to have larger number of flagella²¹ and as a consequence more stator units are turned on. As pH is decreased the faster swimmers suffer an impairment in motor function and their speed shifts to lower values.

The proton concentration in the surrounding medium has a direct effect on the swimming speed of *H. pylori* as it influences the PMF and generates chemoreceptor responses. A change in the transmembrane gradient and the PMF has been associated with various

changes in bacterial motility. As mentioned earlier *E. coli* and *Salmonella* were observed to decrease swimming speeds⁵¹ and motor rotation rates⁵³, while their tumbling is enhanced⁵² in lowered pH environment created by weak acids while *B. subtilis* showed a decrease in both swimming speed and tumbling in low pH⁵⁴. Although the components of the buffer used here, phosphoric acid and succinate acid, have weak acidity, the addition of HCl to change pH complicates the acid penetration. In contrast to these other bacteria, *H. pylori* has evolved to live in an acidic niche. It has sheathed flagella and uses urease to regulate intracellular pH. As shown by the work of Sachs *et al.* in *H. pylori* the pH of the periplasmic space is lowered but not that of the intracellular space due to urease activity. Eventually the flagellar motors do not function well when the intracellular pH becomes too low in agreement with the finding of Sachs *et al.*² who found that transmembrane proton gradient decreases close to zero below pH 3.

The fraction of motile *H. pylori* bacteria also declines with decreasing pH as in the other bacteria mentioned above. Although there are fewer reversals in PGM as compared to broth, the reversal frequency increases at pH 4 in PGM presumably reflecting the effect of gelation at low pH in PGM. Together with the speed distribution analysis, our results suggest that we see a pH-dependence in *H. pylori* swimming speeds and reversal rates providing optimal swimming around pH 5. It is possible that *H. pylori* has adapted to transit through an acidic environment. There is other evidence which supports that *H. pylori* thrives in acidic environment, such as in presence of urea, an acidic environment was necessary for the survival of *H. pylori*⁶⁵ and the urease and metabolic activities of the bacteria increase at pH 4 and below⁶⁶ *H. pylori* is also able to both survive and colonize

deep in the parietal glands⁶⁷ where acid is secreted. Further investigation to reveal the correlation between the transmembrane proton gradient and activation of *TlpB* protein could explain why faster swimming bacteria at lower pH travel in straighter trajectories as shown in our results. It will certainly be an important advance to study the direct correlation and dependence of motility on the transmembrane proton gradient, number of motors, and number of chemoreceptors by examining various mutants and examining the influence of pH on flagella motor proteins at the molecular and biochemical level.

We found that the body rotation rate is only weakly dependent on pH in BB10 but increases in PGM following the viscosity increase as pH decreases below 4. The dropoff in the rotation rate at pH 3 in PGM and BB10 reflects the impairment of flagella motors.

At this low pH many bacteria were coccoidal in both BB10 and PGM indicating that under such extreme acidity bacteria are directly impacted by acid. We showed that in PGM below pH 5 the pH induced effects of increasing viscosity of PGM with decreasing pH take over. At pH above 5, the swimming speed of *H. pylori* decreased slightly as pH increased to 6, reflecting the effect of decreasing pH on flagella as observed in broth.

However, in the absence of urea, the dramatic increase of viscosity below pH 5 starts to constrain the translational movement of the bacteria. The change in speed with pH also correlates with increasing heterogeneity in PGM as pH decreases and viscosity increases.

The gelling of PGM could trap bacteria in liquid pockets (as shown in the confocal images of Figure S2) or the bacteria cell body or flagella can be physically stuck in the gel network (as shown in Figure 3. 5). For stuck bacteria the interaction with the medium could lead to additional forces and torques which hold the bacteria in place and this might

explain the increase in rotational frequency of the cell and loss of translational motion. We also observed that stuck bacteria rotate faster than motile ones, perhaps indicating a mechanosensing ability of *H. pylori* trapped in a gel network. Mechanosensing has been observed in recent studies of the flagellar motor with varying load and viscosity of the medium^{69,70} and they suggest that the bacterial flagellar motor senses external load and mediates the strength of stator binding to the rest of the motor. Our finding of a large variation in rotation frequency and the estimated cell body and motor torque perhaps reflects the viscosity and pH dependent variation in the number of stators activated in *H. pylori*. As discussed earlier, with 18 stators per flagellum^{56,57} and 1-6 flagella in the unipolar bundle of the *H. pylori* strain used here, and as many as 12 flagella in other strains, *H. pylori* has the capacity to vary its motor torque over 2 orders of magnitude and furthermore intracellular pH may directly impact stator binding among other factors. It is an ideal candidate for more detailed studies of pH dependence of torque-speed relationships and the molecular factors governing *H. pylori* motors.

3.5 Conclusions

In conclusion, our findings show that pH has a strong effect on the motility of *H. pylori*, reflecting the competing effects of optimization of flagellar motors to swim faster in slightly acidic media and their immobility in the viscoelastic PGM gel as the bacteria get stuck and cannot translate even though they rotate faster as they mechanosense their environment. A study of speed torque relationship of *H. pylori* as a function of pH would be very interesting, as the system provides an inherent coupling of the pH dependent viscosity of the medium and gelation to effects of pH on motors and receptors. Our

observations have obvious implications for understanding how *H. pylori* is able to breach the gastric mucus barrier and colonize the gastric epithelium, as well as relevance to broader issue of effects of acid in the upper gastrointestinal tract. Measurements of chemotactic motility under pH gradients are currently underway⁶⁵ and provide a more realistic model of relevance to gastric physiology. The results presented here for bacteria swimming in a homogeneous pH environment could further support the development and testing of theoretical and computational models to understand the motion of bacteria in gels and other confined geometries, as well as guide the design of artificial swimmers using pH to control motility.

Chapter 4: Influence of ChePep on Motility of *H. pylori*

Below I am adding a draft of a paper on the effect of protein ChePep on motility of *H. pylori*. The data were acquired by Prof. Bansil's previous student, Maira Constantino. My contribution to this paper is data analysis of all trajectories and calculation of torque and help in writing.

Comparison of run-reverse-reorient motility of Helicobacter pylori and its Δ ChePep mutant reveals higher reversal frequency in the mutant without altering rotation rate or motor torque

Maira A. Constantino^{1,2}, Wentian Liao¹, Manuel Amieva³ and Rama Bansil^{1*},

¹ Boston University, Boston MA 02215

² (current address) National Cancer Institute, Bethesda MD

³ Stanford University Medical Center

4.1 Abstract

The gastric disease-causing bacteria, *Helicobacter pylori* utilize flagella driven motility and chemotaxis to detect external acidic signal as they cross the pH gradient in the viscoelastic, gel-like mucus layer to colonize on the epithelial surface of the stomach. The redirection towards the neutral pH epithelial surface is controlled by the flagellar rotation whose direction is regulated by the phosphorylation and dephosphorylation of protein CheY. Phosphorylated CheY needs to return to non-phosphorylated state by the localization of CheZ in order to be continuously responsive for further directional changing signal. It has been observed that protein ChePep are responsible for the

localization of CheZ and *H. pylori* lacking protein ChePep shows high reversal frequency. Here we present translational and cell body rotational motility data obtained by high resolution, fast frame rate phase contrast microscopy to compare the run speed and turn angle distribution and cell body rotation rate of the wild type (WT) with the Δ ChePep mutant. We also compare our results with theoretical predictions based of run-reversal-reorient motility and resistive force theory calculations of torque. We observe higher reversal frequency of Δ ChePep in agreement with previous observation, however the cell body rotational rate and torque are not influenced by the lack of protein ChePep. Interestingly, both WT and Δ ChePep have maximum probability to maintain their initial run speed after a reorientation or a reversal event, although the distribution indicates that large speed changes are also possible.

4.2 Introduction

Helicobacter pylori (*H. pylori*) is known to survive in harsh environment of human stomach and colonize at the gastric epithelium surface breaching the protective mucus layer of gastric epithelium surface. This colonization can be asymptomatic or lead to gastritis, gastric ulcers and even gastric cancer depending on a variety of host-bacteria interactions. In this paper we focus on motility, which is the first step in getting across the mucus barrier. With regard to motility two of the most important factors which enable the bacteria to go across the viscoelastic mucus barrier which has a pH gradient from 2-4 on the lumen side to neutral on the cell surface. First, *H. pylori* secretes urease which catalyzes the hydrolysis of urea to produce ammonia which will eventually neutralize acid and increase the pH value^{2,3,6}. Previous work from our group has shown that *H.*

pylori are unable to translate even though their flagella rotate when they are in a low pH mucin gel (pH < 4) in the absence of urea. We showed that the increase of pH in the presence of urea triggers a gel-sol transition in the gastric mucin gel creating a liquid environment for *H. pylori* to swim in⁴. Secondly, *H. pylori* employ chemotaxis to distinguish external acidic signal and redirect to the epithelium surface of stomach.

Chemotaxis plays a critical role for the survival of *H. pylori* in the harsh environment of human stomach. For instance, *H. pylori* can distinguish and escape from the low pH environment and further redirect to epithelium surface of stomach which is at neutral pH using pH sensitive chemoreceptors^{7,8,9}. Numerous proteins are involved in this process. First, external pH signals are recognized by chemoreceptor protein TlpB which usually localize at bacterial pole^{10,11}. Chemoreceptor proteins then interact with signaling proteins to amplify the signals¹² and transmit the signal into CheAY through proteins CheW or CheV. CheAY will triggers the phosphorylation of response regulator CheY^{13,14}. Phosphorylated CheY (CheY-P) interacts with flagellar motor and changes the flagellar rotational direction leading the change of bacterial swimming direction. In order to be continuously responsive for external dynamic signal, phosphorylated CheY needs to return to non-phosphorylated state. The dephosphorylation of protein CheY, thus, is vital for the survival of *H. pylori* in a dynamically acidic environment. The dephosphorylation of CheY can either be achieved by its own auto-dephosphorylation or with the help of phosphatases¹⁵. The most-studied phosphatase is CheZ whose localization depends on ChePep. Thus, protein ChePep are thought to improve the dephosphorylation of CheY^{16,17}. Experiments have shown that Δ ChePep shows a 25% decreased colony

diameter in agar plate and 11 times greater reversal frequencies than WT¹⁴ in solution. However, a detailed motility analysis of Δ ChePep has not been done, nor has its flagella or body rotation been examined. By examining the different motility of WT and Δ ChePep, we can better understand what role does protein ChePep play on the chemotaxis and motility of *H. pylori*. Such understanding could be applied on the design of innovative strategy for *H. pylori* therapy.

H. pylori has multiple flagella around its cell body²¹. The flagella at the pole of cell body could form a single flagellar bundle. The counterclockwise rotation of flagella bundle will provide a propulsion to push bacteria forward. The clockwise rotation of flagella bundle will pull bacteria backward. Exactly how the transition from forward to reverse motion occurs is a question of considerable interest. One hypothesis is that between the transition of flagellar bundle rotation direction, flagellar bundle needs to de-bundle first. De-bundling may start from the clockwise rotation of one flagellum of the flagellar bundle causing split of flagellar bundle. When all the flagella start to rotate in the same clockwise rotation direction, a new clockwise rotation bundle formed and bacterial swimming direction changes²². Another possibility is that flagella flip their direction wrapping around the body as has been observed in certain bacteria²³. For certain monotrichous bacteria a run-flick-reverse strategy has been observed²⁴. The trajectories exhibit characteristics of a random walk at long-time scales and this has been explained by the run-tumble model developed by Berg²². In tumble state, without uniform flagellar rotation, barely propulsion is provided by flagellar motor. However, the translational and rotation diffusion can cause slight displacement and body orientation difference. Berg

also founded that by increasing tumble rate, *E. coli* could change their swimming direction more actively to explore more nutritional environment in ocean²⁴. The run-reversal-reorientation model^{18,19,20} are used to describe the motion of *H. pylori* in this paper.

Here, we use phase contrast microscopy at 40X magnification to obtain the swimming trajectories of large number of bacteria. Further analyses allow us to obtain the swimming speed and turn-angle distribution and run-reverse-reorient frequencies, as well as distribution of speed, time and distance traveled between runs (v_{run} , t_{run} , d_{run}). Single bacteria imaging and analysis methods at higher magnification (100X) enable us to measure the cell shape and rotation of cell body to further estimate cell body torque and motor torque, using the methods we developed earlier⁶. We compare the experimental results using the run-reversal-reorientation model^{19,20} to describe the motion of *H. pylori* and further quantitatively analyze the function of protein ChePep in chemotaxis of *H. pylori*. By fitting run time distribution into gamma function³⁴, we can quantitatively analyze the drastic increased reversal frequency of Δ ChePep as compared to WT. From the movies of bacteria at high magnification 100X and high frame rate 100fps, we obtain the cell body rotational rate of WT and Δ ChePep and find that it is almost the same, implying that ChePep does not influence cell body rotation, which is controlled by the flagella motor proteins and number of active flagella and active stators^{69,70}. We also use Resistive Force Theory (RFT) to estimate the cell body and motor torque of both WT and Δ ChePep. The result shows no obvious difference between WT and Δ ChePep on either cell body torque or motor torque.

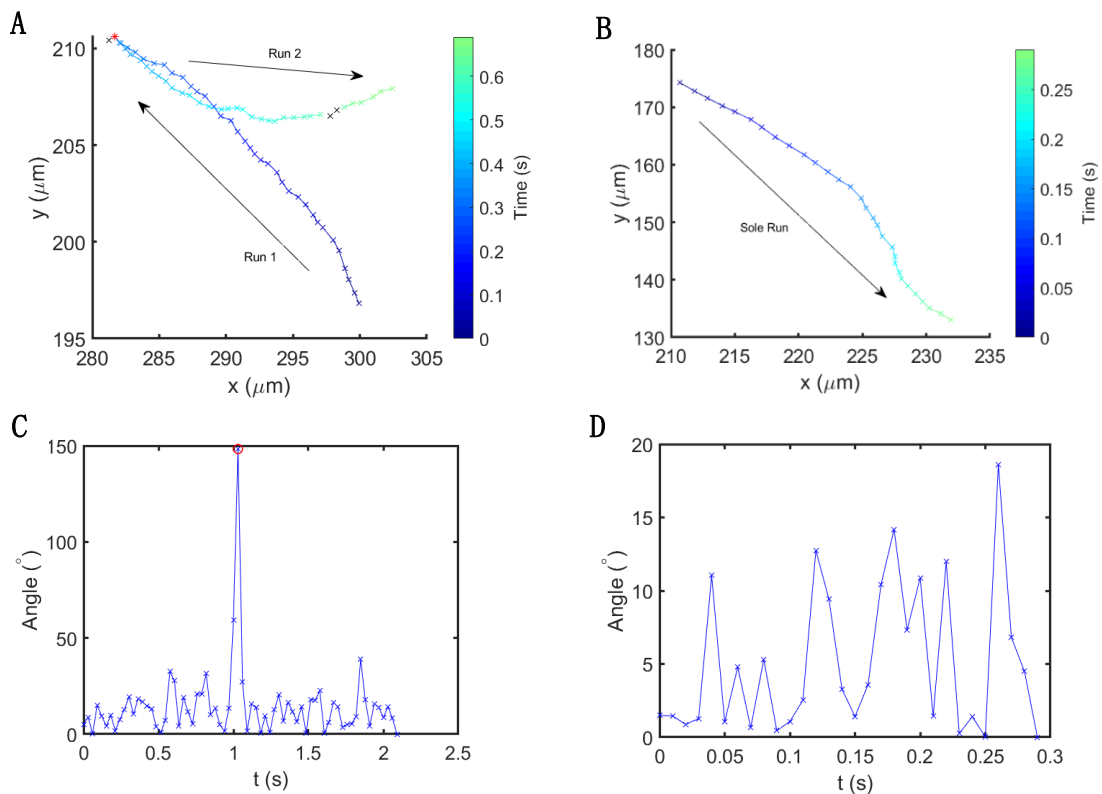
4.3 Results

4.3.1 Super-Diffusive Behavior of Bacteria

In order to study the different swimming behavior of WT and Δ ChePep, we recorded videos of WT and Δ ChePep swimming in broth at 40 X magnification at 33 fps. The bacterial motion of each video is then tracked with the software PolyParticleTracker³⁴ and the trajectory of each bacterium is segmented into runs and reorientations with the method developed by Theves *et al.*³⁴ and Son *et al.*⁷¹. The run segments are identified mainly based on the identification of large alignment angle change and speed change along each trajectory. As shown in Figure 4.1 C, a large alignment angle changed displayed at 1s which correspond to the change of swimming direction of the bacterium in Figure 4. 1A (in red), which eventually leads to two runs of the trajectory. On the other hand, in Figure 4. 1 D, where the alignment angle stays in the range of 0–20°. The swimming trajectory of this bacterium is relatively straight and are considered as one run. For each run, we fit the mean square displacement ($MSD(t) = \langle (\vec{r}(t) - \vec{r}(0))^2 \rangle$) versus time (t) into the power law⁷⁰ $MSD(t) = At^\alpha$. When $\alpha = 1$, particle shows random-walk, diffusive behavior; for $\alpha < 1$, particle shows sub-diffusive behavior; and for $\alpha > 1$, particle shows super-diffusive behavior. Specifically, $\alpha = 2$ corresponds to ballistic motion at constant speed. Particles with self-propulsion ability, like *H. pylori*, will exhibit super-diffusive behavior. Log-log plots of MSD vs time for all trajectories we recorded, are shown in Fig. 3.4. 2 A for the WT (in red) and Δ ChePep (in black). For WT (in red), almost all the trajectories of the MSD vs time plots fit perfectly with the power law with a constant slope of 2 in all time frames. However, for Δ ChePep (in black), there are

obvious zigzag of the plots at the latter part of the plots. The smooth histogram of the α distribution of all trajectories of WT (red) and Δ ChePep (black) can better visualize such difference. As shown in Fig. 4.2 B the WT displays almost ballistic motion with $\alpha = 2$ for about 90% of the trajectories, while Δ ChePep displays a more-or-less uniform distribution of α from 1.2 to 2, indicating that random walk and super-diffusive trajectories are just as likely as ballistic ones.

Figure 4. 1 (A) (B) Trajectories for Δ ChePep with reversal and WT without reversal



respectively. **(C) (D)** Reorientation angle versus time for ChePep with reversal and WT without reversal respectively where the red circle indicates reversal event.

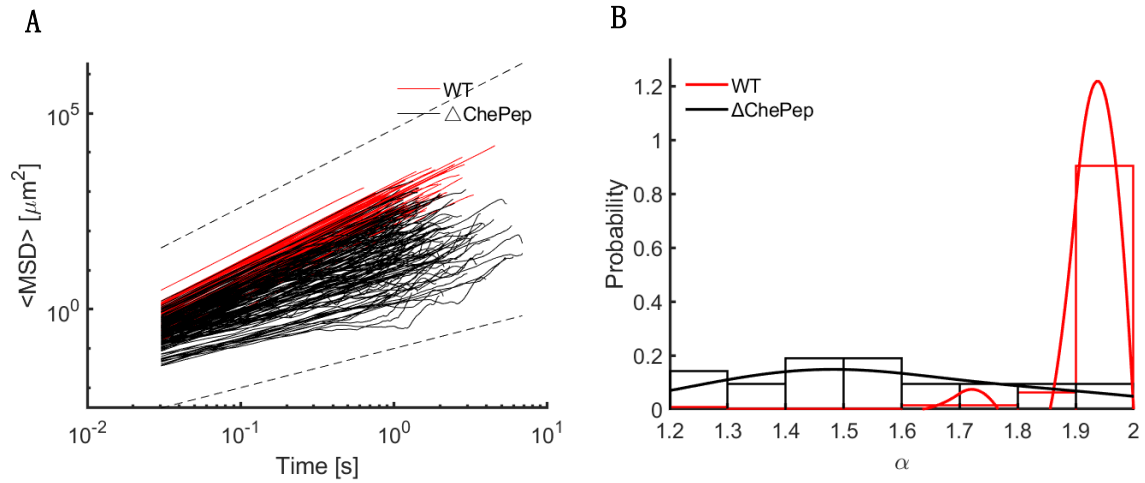


Figure 4. 2 (A) Analysis of MSD vs. time of all trajectories in BB10. Black dash lines are reference lines for $\alpha = 1$ and $\alpha = 2$ (B) Smooth histogram of the α distribution of all trajectories of WT (red) and ΔChePep (black)

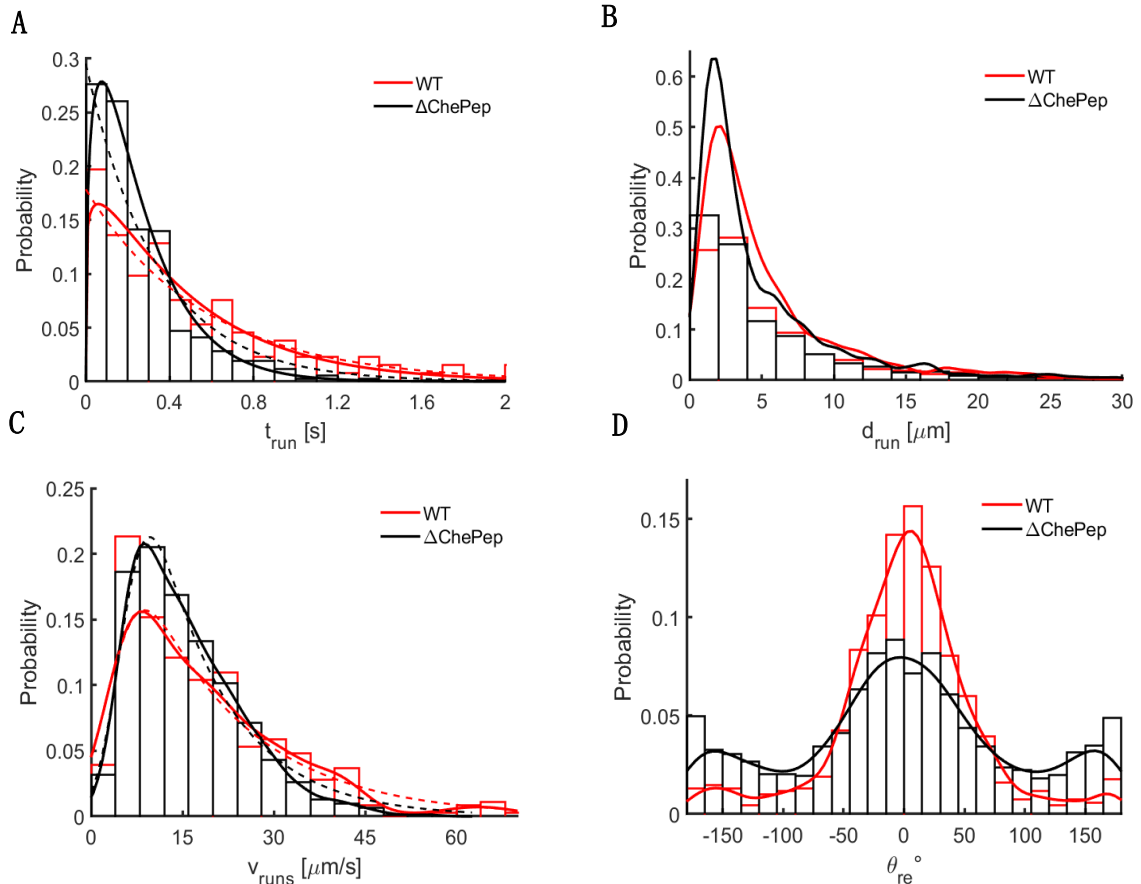
4.3.2 Motility Analysis of WT and Δ ChePep *H. pylori*

Figure 4.3 (A) Smooth histogram of run time distribution of WT (red) and Δ ChePep(black) (B) Smooth histogram of displacement per run distribution of WT (red) and Δ ChePep(black) (C) Smooth histogram of run speed distribution for WT (red)with less reversal and ChePep (black)with more reversal respectively (D) Smooth histogram of the reorientation angle distribution of all trajectories of WT (red) and Δ ChePep (black)

At 40x magnification, significant number of bacteria can be observed, usually up to 100 to 200 bacteria in every video imaged. At least three videos are used for motility analysis including run time, run speed, distance per run, reorientation angle. The run speed (v_{run}) is defined as the average instantaneous speed of each run; The reorientation angle is defined as the turn angle after a reorientation event (θ_{run}). Both WT and Δ ChePep have a

similar run speed distribution from 0 to 70 $\mu\text{m/s}$. The difference is that ΔChePep has a bigger peak of low swimmers while WT has slightly higher probability of faster swimmers. To further characterize the difference of v_{run} on WT and ΔChePep , asymmetric smoothed distribution v_{run} curve was fitted to exponential modified gaussian (EMG) function (in method). Table. 4. 1 summarizes the fitting EMG fitting results clearly shows that WT has both higher mean and median speed but smaller mode.

	mean	std	skew	mode	median
WT	20	17	1.8	8.8	16
ΔChePep	17	12	1.8	9.6	14

Table 4. 1 Mean, standard deviation, skew, median and mode of the average run speeds (v_{run}) and reorientation angle (θ_{re}) of *H. pylori* swimming in BB10.

The reorientation angle distribution of WT and ΔChePep is shown in Fig. 3 (D). Both WT (in red) and ΔChePep in (black) shows a major reorientation peak around $\pm 50^\circ$ and two minor reversal peaks around $\pm 180^\circ$. The difference is that in WT, the reorientation peak dominates contributing more than 90% of reorientation angle change and the two reversal peaks are almost negligible. While for the ΔChePep , the two reversals peak are much more remarkable accounting for more than 30% of the total reorientation angle distribution. The drastic increase of reversal frequency in ΔChePep reveals the malfunction of chemotaxis system of ΔChePep whose flagellar rotation are over-active. The negligible reversals in WT could be result from the flagellar rotational direction response to minute heterogeneity of the medium.

In Figure 4. 3A, run time distribution (t_{run}) of both WT (in red) and Δ ChePep (in black) is smoothed. The smooth distribution of t_{run} share the similar profile with that of v_{run} with a Δ ChePep has a bigger peak at small time and WT are more likely to have longer runs. The difference in run time distribution and reorientation angle distribution can be used synergistically to analyze difference motility behavior of WT and Δ ChePep. The lack of protein ChePep will introduce additional irregular reversals into bacterial trajectory resulting more segments and thus runs of each trajectory, and eventually decrease run time in Δ ChePep. In Figure 4. 3B, distance per run is calculated from the product of run speed to its corresponding run time and smoothed. Similar tendency with run time distribution and run speed distribution is also observed. The relatively bigger peak at small distance may indicate the motile defects of Δ ChePep. Even with the higher reversal frequency, the distance per run of Δ ChePep is smaller than WT. Δ ChePep may be a weak competitor compared with WT since their short run distance will not help me escape from harsh environment and their over-active reversal frequency could be merely a waste of previous energy.

In order to characterize the statistic difference of WT and Δ ChePep t_{run} , d_{run} , v_{run} , θ_{run} . Kolmogorov–Smirnov (K–S) statistics test was performed in MATLAB v. R2019a for t_{run} , d_{run} , v_{run} , θ_{run} respectively, the result shows statistical difference of WT and Δ ChePep in t_{run} , d_{run} , v_{run} , θ_{run} .

t_{run}	d_{run}	v_{run}	θ_{run}
3.16E-08	0.0017	0.0014	9.35E-10

Table 4. 2 p-value of K-S statistics test of the raw data of t_{run} , d_{run} , v_{run} , θ_{run} .

In Figure 4. 3 C, the run speed distribution has broad profile. In order to find the difference on run speed drives from whether the variety of each different bacterium or reorientation reversal events, the relative run speed difference between each consecutive run δV is calculated. The histogram of relative speed difference δV are fitted in to multiple gaussian peaks in Fig. 3.4. 3

$$\delta V = 2 \frac{v_{i+1} - v_i}{v_{i+1} + v_i} \quad (38)$$

Similarly, relative reorientation angle difference between each consecutive run $\delta\theta$ can also be measured.

$$\delta\theta = 2 \frac{\theta_{i+1} - \theta_i}{\theta_{i+1} + \theta_i} \quad (39)$$

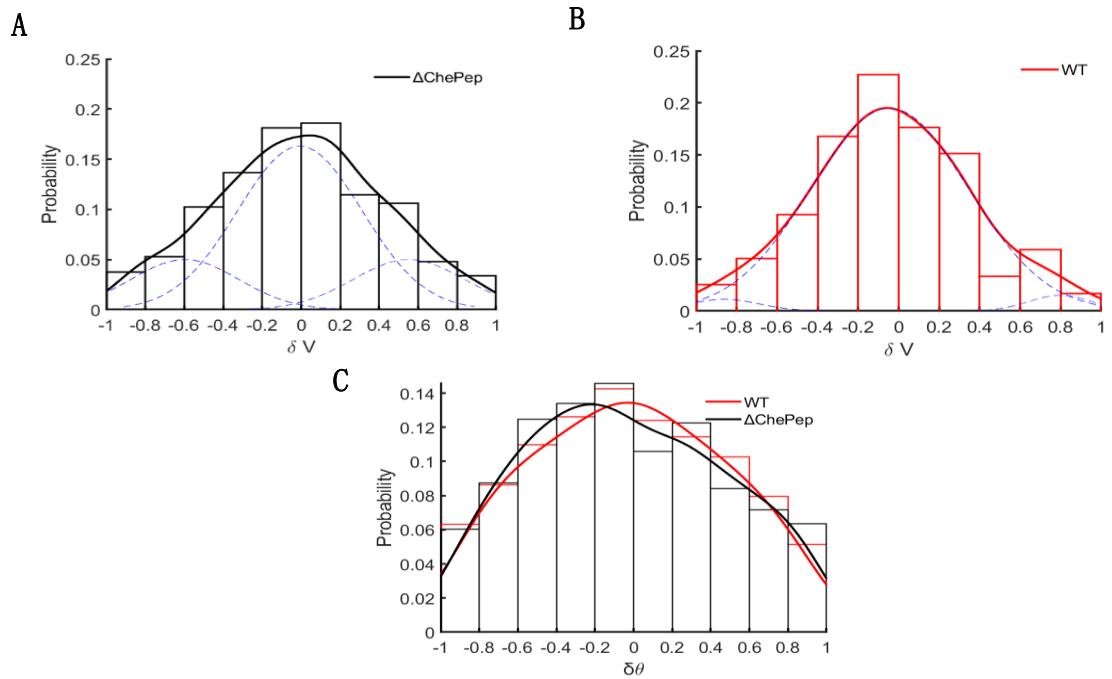


Figure 4. 4 (A) (B) Smooth histogram of relative speed difference of ΔChePep (in black) and WT (in red) respectively. The blue dash line is three gaussian peaks of smooth histogram. **(C)** Smooth histogram of relative reorientation difference of ΔChePep (in black) and WT (in red) respectively

The smooth histogram of δV for ΔChePep (in black) and WT (in red) is displayed in Figure 4. 4 A, B respectively. Both smooth histogram curve shows a dominant peak at around 0 and two minor peaks at two tails. The three different peaks are classified into two categories. The dominant peak at the middle around 0 is the reorientation peak resulting from the negligible run speed difference before and after a reorientation. The two minor peaks at two tails is the reversal peak resulting from the obvious run speed difference between before and after a reversal event.

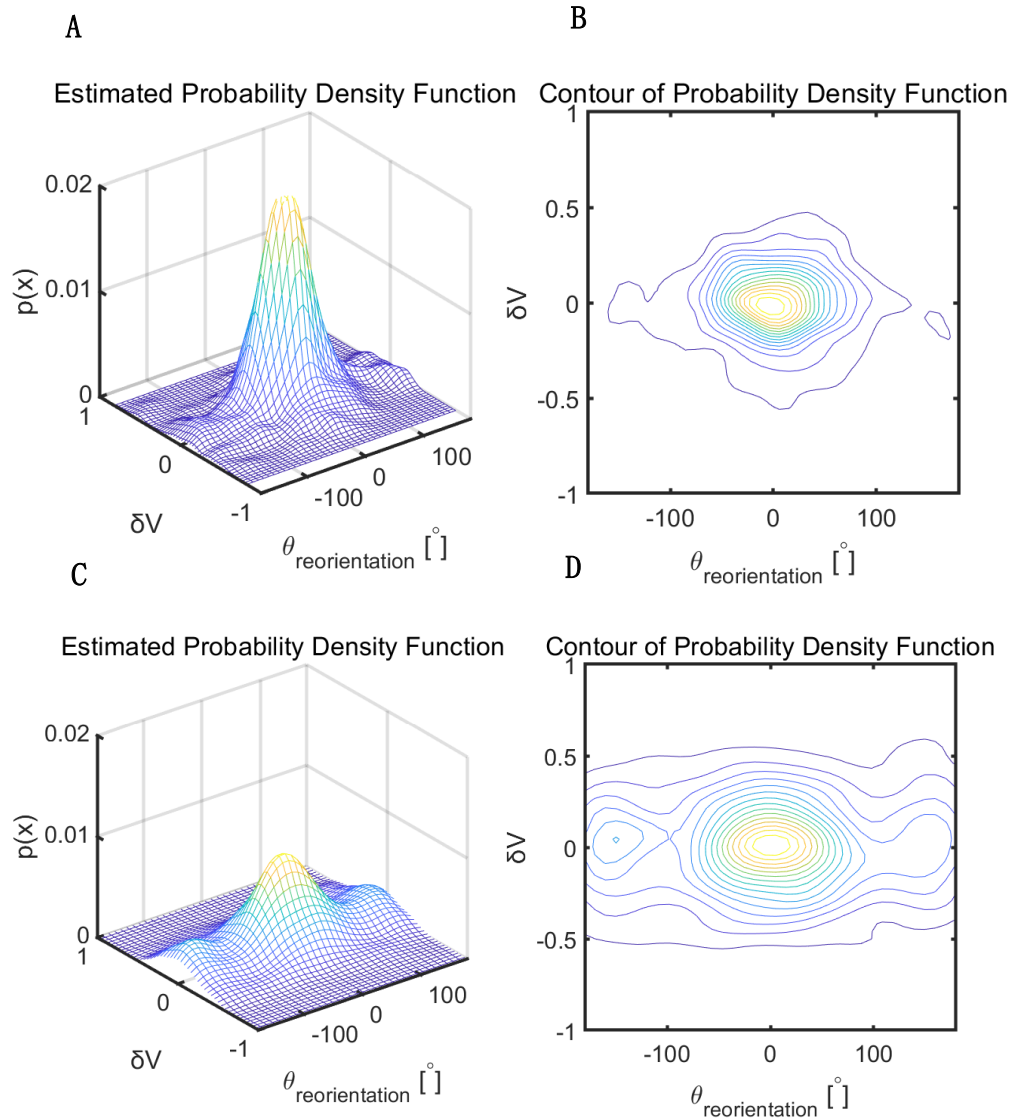


Figure 4.5 (A) (C) Estimated probability density function of reorientation angle (θ) versus δV of WT and Δ ChePep respectively. (B) (D) Contour of probability density function of reorientation angle (θ) versus δV of WT and Δ ChePep respectively.

To further characterize the influence of reorientation angle on run speed difference, the kernel density and contour plot of the reorientation angle (θ) versus relative run speed difference (δV) are presented in Figure 4.5 A, B, C, D. For both WT and Δ ChePep, a reorientation peak locates at small θ with small δV . Such reorientation peak shows that for both WT and Δ ChePep reorientation dominate compared with reversals and

reorientation barely influence run speed. Figure 4.5 C, D shows two additional reversal peaks locate at big θ with small δV for Δ ChePep. The two reversal peaks of Δ ChePep shows an average δV at around 0, which is no consistent with Figure 4.4 A.

It is possible that those bacteria whose reorientation angle is big enough to be considered as reversal still conduct reorientation events. Such reorientation event with large reorientation angle share the same mechanism with normal reorientation event. And those bacteria contribute to $\delta V = 0$ part of the two reversal peaks and obscure the rest with large δV . To illustrate such hypothesis, the distribution of reorientation angle whose δV is in the range of -0.2 to 0.2 is plotted in Figure 4.6 A, B.

In Figure 4. 6 B, the reorientation angle of WT shows a major peak at -50° to 50° and plain for the rest part. While in Figure 4.6 A, except a major peak at -50° to 50° , the reorientation angle of Δ ChePep also shows two minor peaks at high reorientation angle. Thus, the lack of protein ChePep seems not only increase the reversal frequency but also increase the reorientation angle.

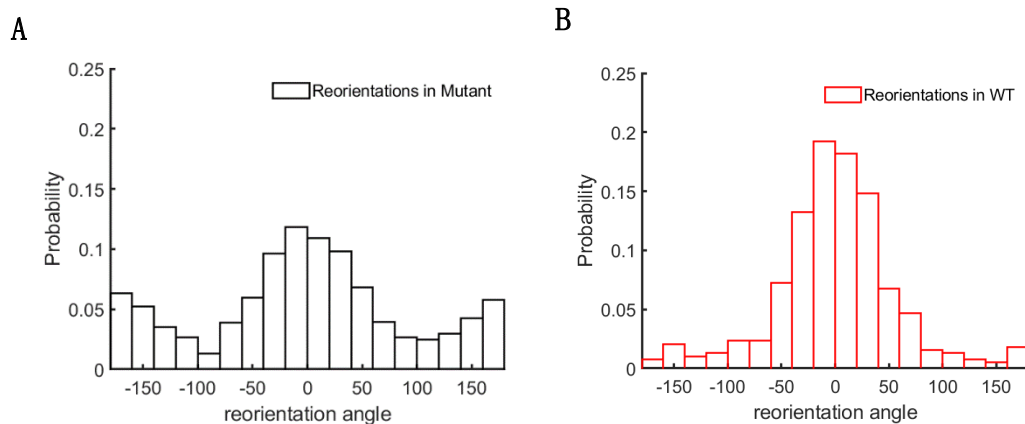


Figure 4. 6 (A) (B) Histogram of reorientation angle (θ) distribution whose δV is in the range of -0.2 to 0.2 for Δ ChePep (in black) and WT (in red) respectively

The run times segmented only by reversals are fitted into probability gamma distribution in the form of the following equation

$$P(t, a, \lambda) = \lambda^a t^{a-1} e^{-\lambda t} / \Gamma(a) \quad (40)$$

where a is the shape factor, λ is the reversal rate. And therefore, reversal frequency $\omega = \lambda/a$. The following table 2 is the a and λ for WT and Δ ChePep respectively.

	a	λ	ω
WT	1	0.05	0.05
ΔChePep	0.4	0.13	0.0325

Table 4.3 The parameters of a gamma function fit to the probability distribution data for t_{run} shown in Fig. 3.4. 2, where $P(t, a, \lambda) = \lambda^a t^{a-1} e^{-\lambda t} / \Gamma(a)$.

The reversal frequency of Δ ChePep is more than ten times of that of WT.

4.3.3 Body Rotation Analysis of WT and Δ ChePep *H. pylori* and Resistive Force Theory

In order to test whether the lack of protein ChePep will influence the cell body rotation of *H. pylori* WT and Δ ChePep are imaged at 100X magnification and 100 fps following Celltool^{®6} analysis. The results include cell body rotation rate, geometrical parameters, accurate translational speed. Figure 4.7A, B, C show the cell body rotation rate (Ω), translational speed (V) and distance per rotation (V/Ω) of WT (in red) and Δ ChePep (in black). The cell body rotational rate is almost the same for WT and Δ ChePep, while WT shows a slightly higher translational speed than Δ ChePep which coincide with the run speed distribution in Figure 4.3C. Figure 4.7 D, E is the cell body torque and motor torque estimated using Resistive Force Theory. Cell body torque is calculated from

Resistive Force Theory (RFT) as briefly described by Magariyama *et al.*³⁵. Motor torque is estimated from the helical model developed by Martinze¹⁸ an improvement of Magariyama's ellipsoidal body shape model. Briefly, RFT states that at low Reynolds number a rotating flagellum produce an axial thrust F and torque T which is related to the flagellum's axial velocity V and rotation rate Ω ²⁸.

$$\begin{pmatrix} F \\ T \end{pmatrix} = \begin{pmatrix} A_{11} & A_{12} \\ A_{12} & A_{22} \end{pmatrix} \begin{pmatrix} V \\ \Omega \end{pmatrix} \quad (41)$$

where the 2x2 matrix depends on the geometric parameters of the cell body or flagella. For helical body shape, $T = A_{12}V + A_{22}\Omega$ where A_{12} is the translational drag coefficient (α) and A_{22} is the rotational drag coefficient (β). While for ellipsoidal body shape, $T = A_{22}\Omega$ since A_{12} vanish. Thus, cell body torque and flagellar torque could be estimated from ellipsoidal or helical body parameters and rotation and translational speed recorded from Celltool^{®35} analysis. Due to the balance of flagellar torque and motor torque, we could estimate motor torque from flagellar torque. However, limitation of RFT exist due to its assumption of decoupling, torque balance and the assumption that cell body and

flagellar bundle are colinear. A more reliable torque estimation could be done through Regularized Stokeslet model³⁸.

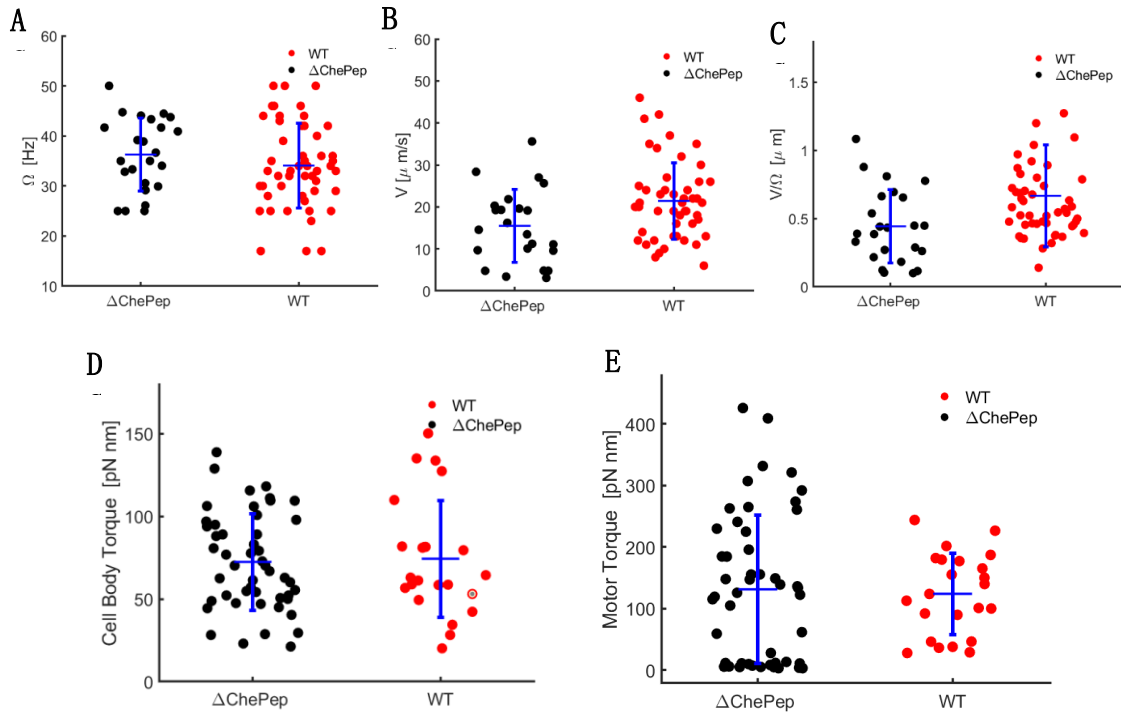


Figure 4.7 (A) Scatter plot of the cell body rotational rate (Ω) for WT (in red) and Δ ChePep (in black) respectively. (B) Scatter plot of the translational speed (V) for WT (in red) and Δ ChePep (in black) respectively. (C) Scatter plot of the V/Ω for WT (in red) and Δ ChePep (in black) respectively. (D) Scatter plot of cell body torque for WT (in red) and Δ ChePep (in black) respectively. (E) Scatter plot of motor torque for WT (in red) and Δ ChePep (in black) respectively

With the large polydispersity of cell body parameter of each bacterium imaged, both WT and Δ ChePep shows a distribution of both cell body torque and motor torque. Even though, the cell body torque and motor torque for WT and Δ ChePep are almost identical indicating that the lack of protein of ChePep does not influence in general either the cell body rotation or the flagellar bundle rotation.

4.4 Discussion

We have compared the different motility behavior and cell body rotation of WT and Δ ChePep. Our results show that Δ ChePep intend to have a more than 10 times higher reversal frequency than WT indicating the malfunction of Δ ChePep chemotaxis. Such defect can be deadly for the competition of Δ ChePep with WT. With this dysfunctional chemotaxis system, Δ ChePep will lose its precious energy during frequent and meaningless reversals. Potential *H. pylori* therapy could be the trigger of Δ ChePep mutation of WT. In human stomach, Δ ChePep is less competitive than WT since their abnormally high reversal frequency may redirect them into harsh luminal stomach instead of escaping from it like WT. However, the acid presented in human stomach may also influence the reversal frequency of Δ ChePep. Thus, further experiment on the motility of Δ ChePep in PGM in different is required for further testify the potential of Δ ChePep mutation trigger technique as *H. pylori* therapy.

The average swimming speed of WT and Δ ChePep are roughly the same in both 100X and 40X results revealing that the flagellar motor efficiency is not influenced by the lack of protein ChePep during each run state. However, from the MSD versus time plots, it is obvious that ballistic motion is dominant in WT while Δ ChePep show no preference on neither super-diffusive behavior nor ballistic motion. The swimming speed of WT is also higher than that of Δ ChePep in both 100X and 40X magnification movies. This typical trend that a ballistic motion usually have a higher speed is similar to that of Constantino *et al.*'s observation on the bipolar *H. suis*²³ bacterium where the bacterium with one flagellum extended and one wrapped swam the fastest and displayed ballistic trajectories

while those with both flagella wrapped displayed super-diffusive random walk trajectories and slower swimming speed.

The smooth histogram of relative speed difference is fitted into multiple gaussian peaks. Both WT and Δ ChePep display a dominant peak at around 0 with two minor peaks at tail. Its difference is the magnitude of the two minor peaks in corresponding curves. The two minor peaks in Δ ChePep are obviously outstrip the two minor peaks in WT indicating Δ ChePep are more likely to change its speed after a reorientation or reversals. In order to figure out whether reorientation or reversal contribute the two peaks, the scatter plot of reorientation angle (θ) versus relative speed difference (δV) is presented in Figure 4. 5 A, B, E, F. Both in WT and Δ ChePep, δV concentrate at around 0 in almost all reorientation angle including both reorientation and reversal. The concentration of δV at 0 coincide with the major peak of smooth histogram curve of δV . But not only reorientation but also reversal contribute this major peak. Thus, after the reversal the speed could maintain relatively the same with before the reversal. It is possible that those bacteria whose reorientation angle is big enough to be considered as reversal still conduct reorientation events. Such reorientation event with large reorientation angle share the same mechanism with normal reorientation event. The only difference is the magnitude of the reorientation angle.

In Figure 4. 6 B, only one major peak shows up from -50° to 50° . Such distribution coincides with previous hypothesis that reversal with large reorientation angle lead to larger δV and reorientation with small reorientation angle lead to small δV . However, in

Figure 4. 6A, two additional reorientation peaks at large reorientation angle indicate that the lack of protein ChePep may also increase the magnitude of reorientation event with large reorientation angle. Therefore, Δ ChePep not only has increased the reversal frequency but also increased the reorientation event with large reorientation angle. Therefore, the lack of protein ChePep will first increase the flagellar de-bundle frequency and therefore Δ ChePep shows increased reorientation frequency. After the flagellar re-bundle, the flagellar rotational direction does not necessary change leading various δV distribution.

By the measurement of the cell body rotation rate and estimation of cell body torque and motor torque, the influence of the lack of protein ChePep on cell body rotation and flagellar motor rotation is precluded. In Figure 4.7A, the cell body rotation rate measured for WT and Δ ChePep are relatively the same at around 35 Hz. And the cell body torque calculated is also 350 pN nm in both WT and Δ ChePep as shown in Figure 4.7 C. The motor torque is estimated from $T_m = v_h/S_h$ and no obvious difference is observed from Figure 4.7D. We use the same flagellar rotation frequency and flagellar bundle parameters obtained from Constantino³⁶ for all the motor torque estimation. We may obscure the influence the lack of protein ChePep on the rotational frequency or geometric parameters of flagella bundle. But overall, the lack of protein ChePep are observed to only influence the speed rather than cell body rotation rate.

4.5 Conclusions

The redirection towards the neutral pH epithelial surface is controlled by the flagellar rotation whose direction is regulated by the phosphorylation and dephosphorylation of protein CheY. Phosphorylated CheY needs to return to non-phosphorylated state by the localization of CheZ in order to be continuously responsive for further directional changing signal. It has been observed that protein ChePep are responsible for the localization of CheZ and *H. pylori* lacking protein ChePep shows high reversal frequency. Here we present translational and cell body rotational motility data obtained by high resolution, fast frame rate phase contrast microscopy to compare the run speed and turn angle distribution and cell body rotation rate of the wild type (WT) with the Δ ChePep mutant. We also compare our results with theoretical predictions based of run-reversal-reorient motility and resistive force theory calculations of torque. We observe higher reversal frequency of Δ ChePep in agreement with previous observation, however the cell body rotational rate and torque are not influenced by the lack of protein ChePep. Interestingly, both WT and Δ ChePep have maximum probability to maintain their initial run speed after a reorientation or a reversal event, although the distribution indicates that large speed changes are also possible.

Supplementary Information

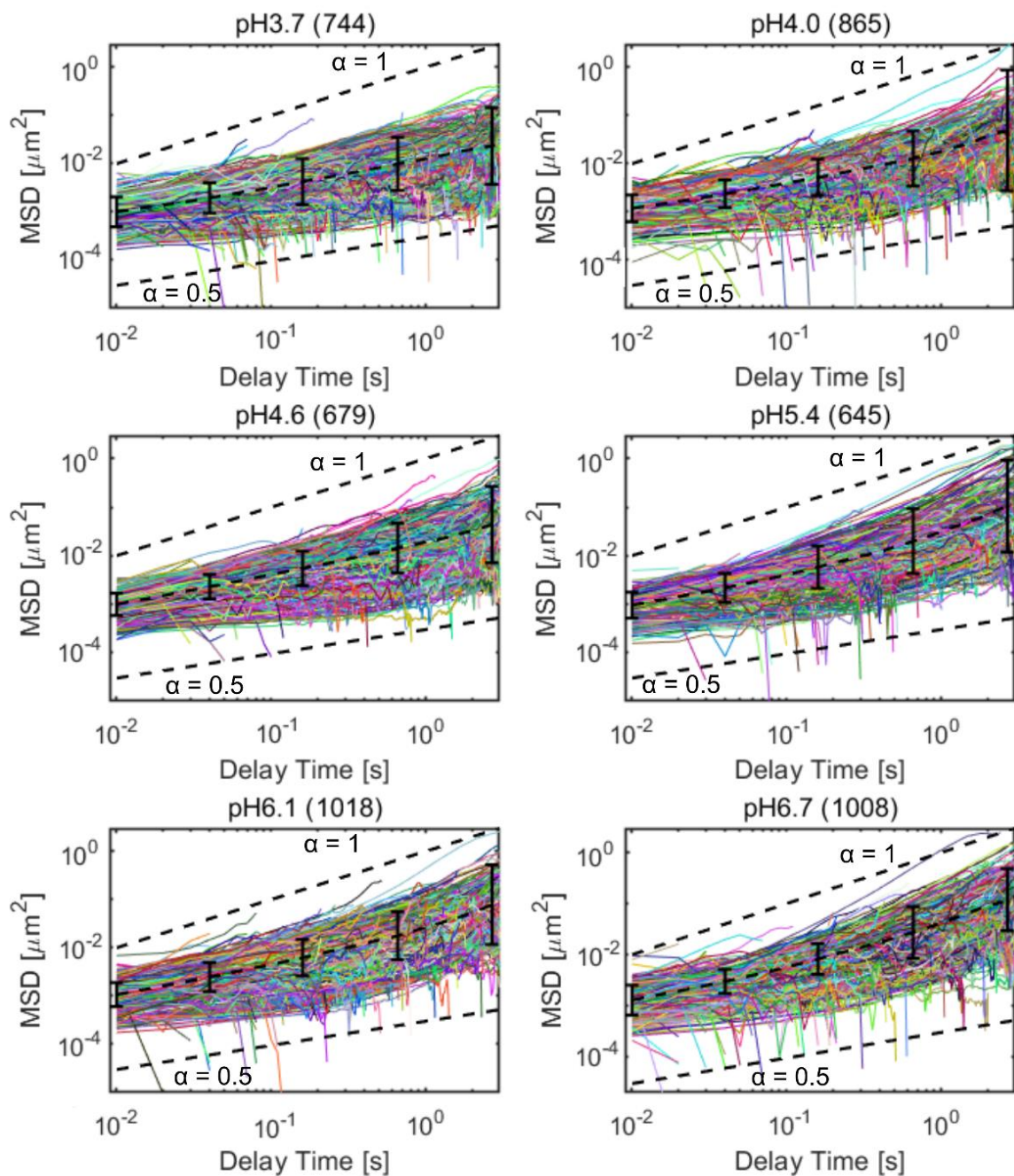


Figure. S1 A All particle MSD vs delay time in BB10 at different pHs as indicated. The average $\langle \text{MSD} \rangle$ and relative error of log MSD defined as $\varepsilon = \pm 0.436 \sigma_{\text{MSD}} / \langle \text{MSD} \rangle$ are displayed by the black line and error bars. Numbers in parenthesis on pH legends indicate number of particles tracked.

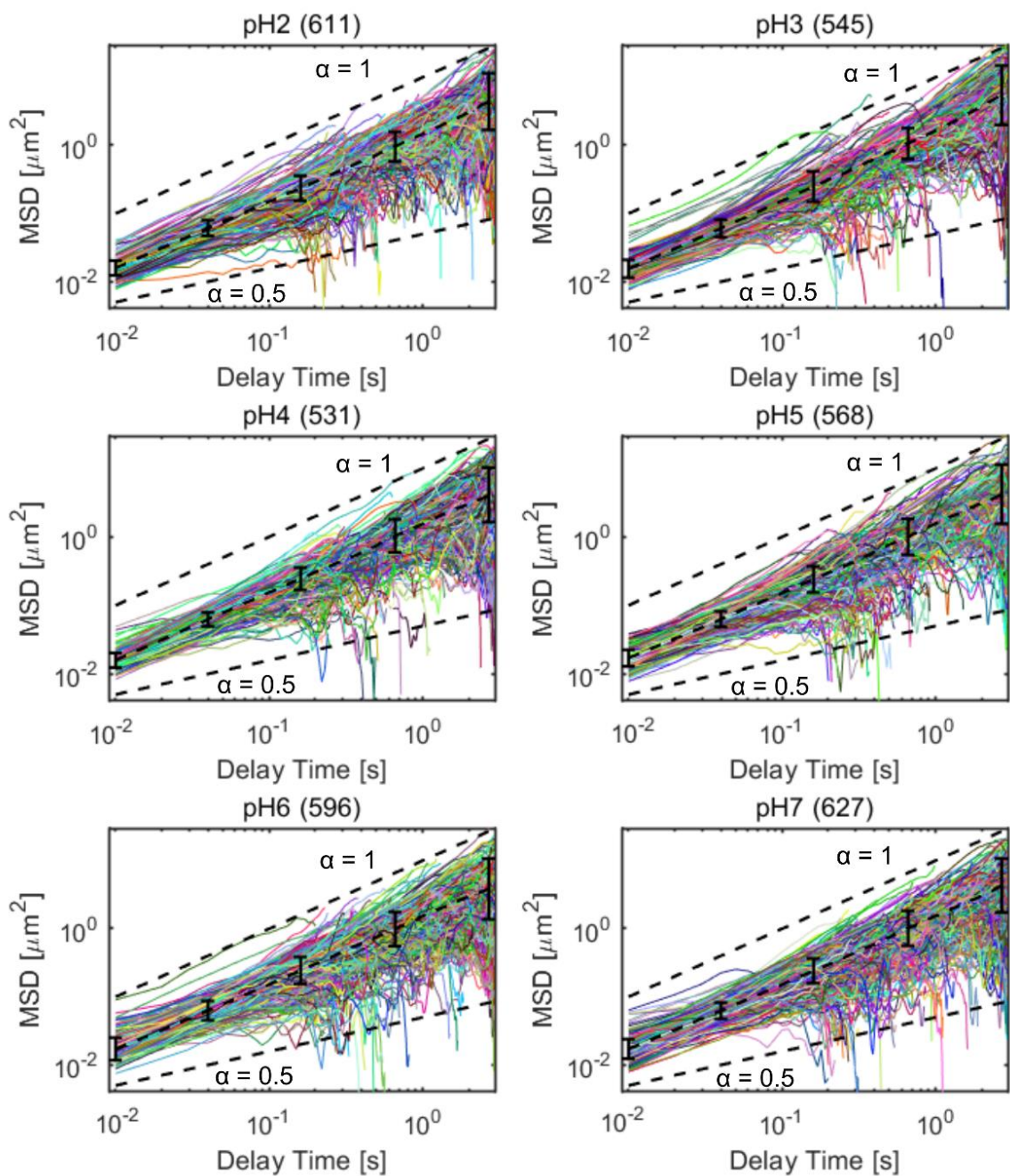


Figure. S1 B. All particle MSD vs delay time in PGM at different pHs as indicated on a log-log plot. The average $\langle \text{MSD} \rangle$ and relative error of log MSD defined as $\varepsilon = \pm 0.436 \sigma_{\text{MSD}} / \langle \text{MSD} \rangle$ are displayed by the black line and error bars. Numbers in parenthesis on pH legends indicate number of particles tracked.

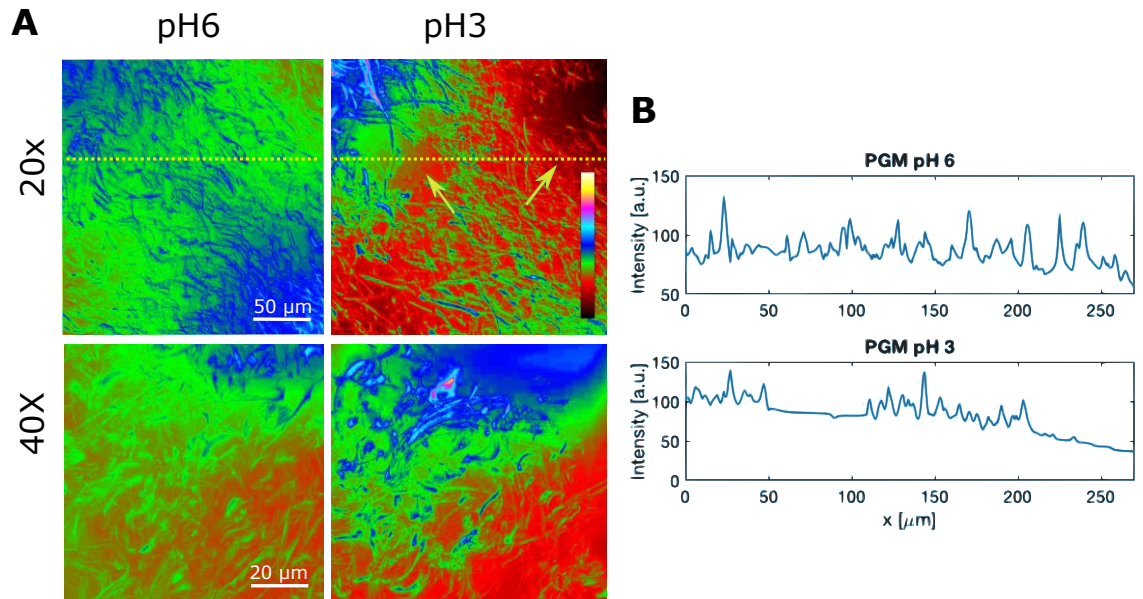


Figure S2 Confocal DIC microscopy images of PGM solution at pH 6 and gel at pH 3. (A) Images at 20X and 40X objective magnifications at pH 6 and 3. The mucin strands are displayed as bright green to blue on the aqueous background indicated by low intensity regions colored in red (see color scale bar on top right). The arrows in the 20X image of PGM at pH3 point to liquid regions with little mucin. (B) The intensity profile measured across the image along the line indicated in yellow in (A).

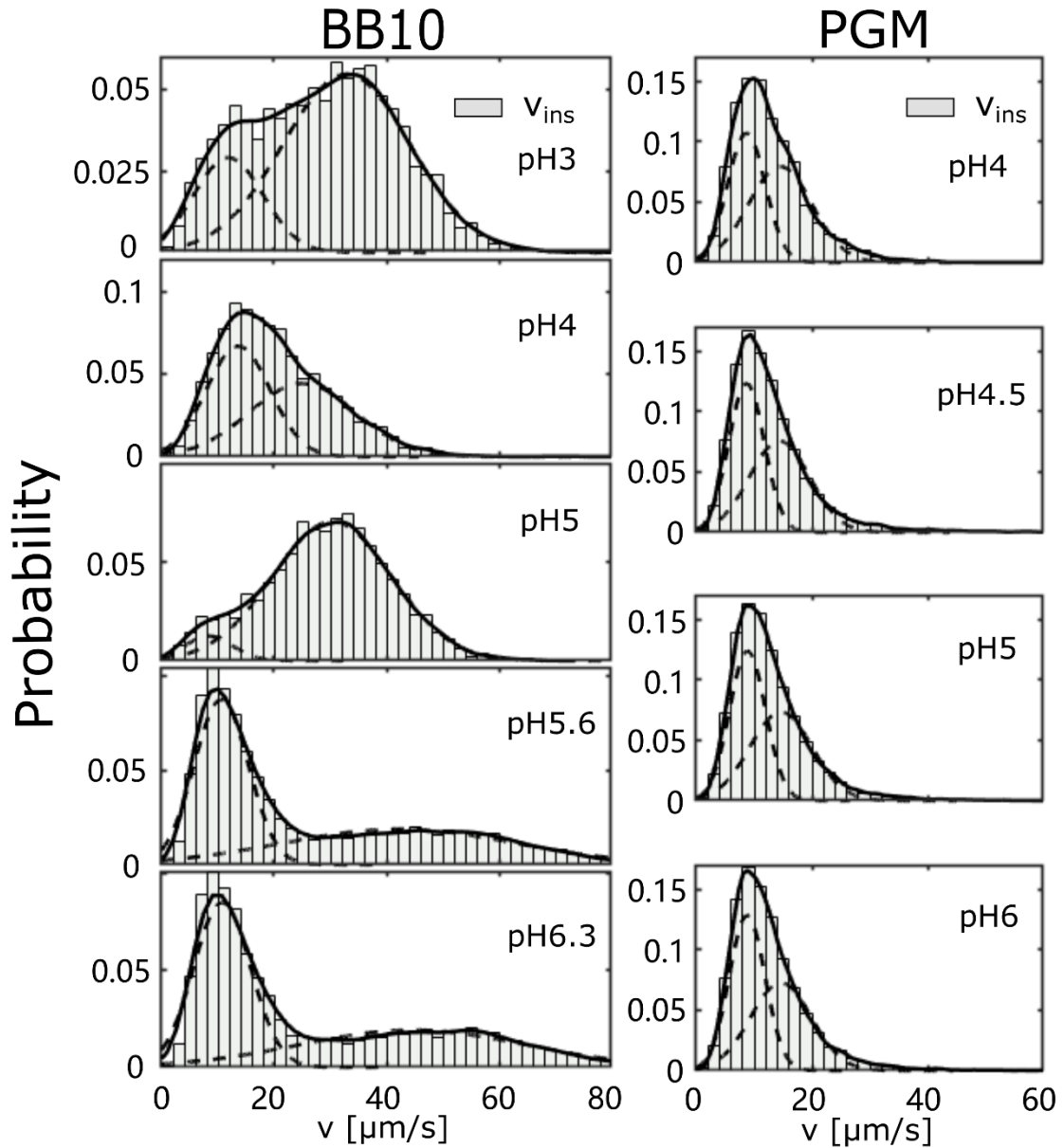


Figure S3 Two peak fit of distribution of instantaneous speeds, v_{inst} for J99 *H. pylori* bacteria swimming in BB10 and PGM at different pHs as indicated. The number of motile trajectories that were analyzed ranges from 185 at pH 4 to 388 at pH 3 in BB10 and from 136 at pH 4 to 625 at pH 4.5 in PGM.

Medium	pH	slow peak				fast peak			
		amplitude	position	width	area	amplitude	position	width	area
PGM	4	0.11	8.67	4.60	0.44	0.08	14.52	7.77	0.56
	4.5	0.12	8.68	4.36	0.49	0.08	14.39	7.36	0.51
	5	0.12	8.86	4.43	0.50	0.07	14.64	7.60	0.50
	6	0.13	8.79	4.40	0.51	0.07	14.64	7.46	0.49
BB10		slow peak				fast peak			
		amplitude	position	width	area	amplitude	position	width	area
	3	0.03	11.87	8.79	0.23	0.05	32.88	16.04	0.77
	4	0.07	13.63	8.03	0.48	0.04	25.04	13.35	0.52
	5	0.01	8.39	5.98	0.07	0.07	30.33	14.98	0.93
	5.6	0.09	10.60	6.84	0.52	0.02	42.31	29.41	0.48
	6.3	0.08	10.75	7.18	0.53	0.02	44.65	28.47	0.47

Table. S1 Summary of 2 peak fit. The parameters of the 2 Gaussian peaks for v_{inst} and v_{run} speed distributions in PGM and BB10 at different pH. The fit function is given in Methods and width = $\sqrt{2} \sigma$.

Bibliography

1. Salama, N., Shepherd, B. and Falkow, S. (2004). Global Transposon Mutagenesis and Essential Gene Analysis of *Helicobacter pylori*. *Journal of Bacteriology*, 186(23), 7926-7935.
2. Sachs, G., Weeks, D., Wen, Y., Marcus, E., Scott, D. and Melchers, K. (2005). Acid Acclimation by *Helicobacter pylori*. *Physiology*, 20(6), 429-438.
3. Sidebotham, R. L., Worku, M. L., Karim, Q. N., Dhir, N. K., Baron, J. H. (2003). How *Helicobacter pylori* urease may affect external pH and influence growth and motility in the mucus environment. *EMBO Journal*, 15(4), 395–401.
4. Montecucco, C., Rappuoli, R. (2001). Living dangerously: How *Helicobacter pylori* survives in the human stomach. *Nature Reviews. Molecular Cell Biology*, 2(6), 457–466
5. Celli, J. P., *et al.* (2009). *Helicobacter pylori* moves through mucus by reducing mucin viscoelasticity. *Proceedings of the National Academy of Sciences of the United States of America*, 106(34), 14321–14326.
6. Su, C, *et al.* (2019). Intrinsic swimming dynamics influences motility of *H. pylori* under acidic conditions and sol-gel rheology of mucin manifests in mechanosensing the gel, *Science Advances*, in press.
7. Foynes, S., Dorrell, N., Ward, S. J., Stabler, R. A., McColm, A. A., Rycroft, A. N., Wren, B. W. (2000). *Helicobacter pylori* possesses two CheY response regulators and a histidine kinase sensor, CheA, which are essential for chemotaxis and colonization of the gastric mucosa. *Infection and Immunity*, 68(4), 2016–2023.

8. Terry, K., Williams, S. M., Connolly, L., Ottemann, K. M. (2005). Chemotaxis plays multiple roles during *Helicobacter pylori* animal infection. *Infection and Immunity*, 73(2), 803–811.
9. Lertsethtakarn, P., Ottemann, K. M., Hendrixson, D. R. (2011). Motility and chemotaxis in Campylobacter and Helicobacter. *Annual Review of Microbiology*, 65, 389–410.
10. Croxen, M. A., Sisson, G., Melano, R., Hoffman, P. S. (2006). The *Helicobacter pylori* chemotaxis receptor TlpB (HP0103) is required for pH taxis and for colonization of the gastric mucosa. *Journal of Bacteriology*, 188(7), 2656–2665.
11. Goers Sweeney, E., Henderson, J. N., Goers, J., Wreden, C., Hicks, K. G., Foster, J. K., ... Guillemin, K. (2012). Structure and proposed mechanism for the pH-sensing *Helicobacter pylori* chemoreceptor TlpB. *Structure*, 20(7), 1177–1188.
12. Sourjik, V., Armitage, J. P. (2010). Spatial organization in bacterial chemotaxis. *EMBO Journal*, 29(16), 2724–2733.
13. Jiménez-Pearson, MA., Delany, I., Scarlato, V., Beier, D. (2005). Phosphate flow in the chemotactic response system of *Helicobacter pylori*. *Microbiology*, 151(10), 3299–3311.
14. Lertsethtakarn, P., Ottemann, K. M. (2010). A remote CheZ orthologue retains phosphatase function. *Molecular Microbiology*, 77(1), 225–235.
15. Howitt, M. R., Lee, J. Y., Lertsethtakarn, P., Vogelmann, R., Joubert, L. M., Ottemann, K. M., Amieva, M. R. (2011). ChePep controls *Helicobacter pylori* Infection of the gastric glands and chemotaxis in the Epsilonproteobacteria.

- Molecular Biology*, 2(4), e00098-11.
16. Wadhams, G., Armitage, J. (2004). Making sense of it all: bacterial chemotaxis. *Nature Reviews. Molecular Cell Biology*, 5(12), 1024–1037.
 17. Silversmith, R. E. (2010). Auxiliary phosphatases in two-component signal transduction. *Current Opinion in Microbiology*, 13(2), 177–183.
 18. Martínez, L. E., Hardcastle, J. M., Wang, J., Pincus, Z., Tsang, J., Hoover, T. R., Salama, N. R. (2016). *Helicobacter pylori* strains vary cell shape and flagellum number to maintain robust motility in viscous environments. *Molecular Microbiology*, 99(1), 88–110.
 19. Lowenthal, A. C., Hill, M., Sycuro, L. K., Mehmood, K., Salama, N. R., Ottemann, K. M. (2009). Functional analysis of the *Helicobacter pylori* flagellar switch proteins. *Journal of Bacteriology*, 191(23), 7147–7156.
 20. Schweinitzer, T., Mizote, T., Ishikawa, N., *et al.* (2008). Functional characterization and mutagenesis of the proposed behavioral sensor TlpD of *Helicobacter pylori*. *Journal of Bacteriology*, 190(9), 3244–3255.
 21. Constantino, M.A. (2017). Investigating effects of morphology and flagella dynamics on swimming kinematics of different helicobacter species using single-cell imaging. Doctoral Dissertation, Boston University.
<https://open.bu.edu/handle/2144/27383>
 22. Berg, H., Brown, D. (1972). Chemotaxis in *Escherichia coli* analysed by Three-dimensional Tracking. *Nature*, 239(5374), 500–504

23. Constantino, M.A., Jabbarzadeh, M., Fu, H.C. *et al.* (2018). Bipolar lophotrichous *Helicobacter suis* combine extended and wrapped flagella bundles to exhibit multiple modes of motility. *Scientific Reports*, 8, 14415
24. Xie, L., Altindal, T., Chattopadhyay, S., Wu, X. (2011). Bacterial flagellum as a propeller and as a rudder for efficient chemotaxis. *Proceedings of the National Academy of Sciences of the United States of America*, 108(6), 2246-2251.
25. Berg, H. C., Tedesco, P. M. (1975). Transient response to chemotactic stimuli in *Escherichia coli*. *Proceedings of the National Academy of Sciences of the United States of America*, 72(8), 3235–3239.
26. Berg, H. C. (1993). *Random walks in biology*. Princeton University Press.
27. Purcell, E. M. (1977). Life at low Reynolds number. *American Journal of Physiology*, 45(1), 3–11
28. Rodenborn, B., Chen, C. H., Swinney, H. L., Liu, B., Zhang, H. P. (2013). Propulsion of microorganisms by a helical flagellum. *Proceedings of the National Academy of Sciences of the United States of America*, 110 (5) E338-E347.
29. Pincus, Z., Theriot, J. A. (2007). Comparison of quantitative methods for cell-shape analysis. *Journal of Microscopy*, 227(2), 140–156.
30. Gray, J., and Hancock, G. (1955). The propulsion of sea-urchin spermatozoa. *Journal of Experimental Biology*, 32(4), 802–814.
31. Cortez, R., Fauci, L., and Medovikov, A. (2005). The method of regularized Stokeslets in three dimensions: analysis, validation, and application to helical swimming. *Physics of Fluids*, 17(3), 031504-031510.

32. Su, Clover. (2019). Influence of Acid on Motility and Chemotactic Response of *Helicobacter pylori* in Gastric Mucin. Doctoral Dissertation, Boston University.
<https://open.bu.edu/handle/2144/36152>
33. Rogers, S. S., Waigh, T. A., Zhao, X. Lu, J. R. (2007). Precise Particle Tracking Against a Complicated Background: Polynomial Fitting with Gaussian Weight. *Physical Biology*, 4(3), 220–227.
34. Theves, M., Taktikos, J., Zaburdaev, V., Stark, H., Beta, C. (2013). A bacterial swimmer with two alternating speeds of propagation. *Biophysical Journal*, 105(8), 1915–1924
35. Schneider, C. A, Rasband, W. S. Eliceiri, K. W. (2012), NIH Image to ImageJ: 25 years of image analysis. *Nature Methods*, 9(7): 671-675.
36. Constantino, M. A., Jabbarzadeh, M., Fu, H. C., Bansil, R. (2016). Helical and rod-shaped bacteria swim in helical trajectories with little additional propulsion from helical shape. *Science Advances*, 2(11), e1601661.
37. Massey, F. J. (1951). The Kolmogorov-Smirnov Test for Goodness of Fit. *Journal of the American Statistical Association*, 46(253), 68–78.
38. Hill, P. D. (1985). Kernel estimation of a distribution function. *Communications in Statistics - Theory and Methods*. 14(3), 605-620.
39. Grushka, Eli. (1972). Characterization of exponentially modified Gaussian peaks in chromatography. *Analytical Chemistry*, 44(11), 1733–1738.
40. Hollander, F. (1954). The two-component mucous barrier; its activity in protecting the gastroduodenal mucosa against peptic ulceration. *Archives of Internal*

- Medicine*, 93(1), 107–129.
41. Kauffman, G. L. J. (1981). Gastric mucus and bicarbonate secretion in relation to mucosal protection. *Journal of Clinical Gastroenterology*, 21(3), 45–50.
 42. Davenport, H. W. (1958). *The ABC of Acid-base Chemistry*, 4th ed. Chicago Press.
 43. Fimmel, C. J., Etienne, A., Cilluffo, T. (1985). Long-term ambulatory gastric pH monitoring: Validation of a new method and effect of H₂-antagonists. *Gastroenterology*, 88(6), 1842–1851.
 44. Ayazi, S., M. Leers, J., Oezcelik, A., Abate, E., Peyre, C. G. (2009). Measurement of gastric pH in ambulatory esophageal pH monitoring. *Surgical Endoscopy and Other Interventional Techniques*, 23(9), 1968–1973 .
 45. Cao, X., Bansil, R., Bhaskar, K. R., Turner, B. S., LaMont, J. T., Niu, N., Afdhal, N. H. (1999). pH-dependent conformational change of gastric mucin leads to sol-gel transition. *Biophysical Journal*, 76(3), 1250–1258.
 46. Celli, J. P., Turner, B. S., Afdhal, N. H., Ewoldt, R. H., Mckinley, G. H., Bansil, R., Erramilli, S. (2007). Rheology of gastric mucin exhibits a pH-dependent sol-gel transition. *Biomacromolecules*, 8(5), 1580–86.
 47. Maixner, F., Krause-Kyora, B., Turaev, D., Herbig, A., Hoopmann, M. R., Hallows, J. L., Zink, A. (2016). The 5300-year-old *Helicobacter pylori* genome of the Iceman. *Science*, 351(6269), 162–165.
 48. Bansil, R., Celli, J. P., Hardcastle, J. M., Turner, B. S. (2013). The Influence of Mucus Microstructure and Rheology in *Helicobacter pylori* Infection. *Frontiers in Immunology*, 2013(4), 310-322.

49. Manson, M. D., Tedesco, P., Berg, H. C., Harold, F. M., Van der Drift, C. (1977). A protonmotive force drives bacterial flagella. *Proceedings of the National Academy of Sciences of the United States of America*, 74(7), 3060–3064.
50. Wen, Y., Scott, D. R., Vagin, O., Tokhtaeva, E., Marcus, E. A., Sachs, G. (2018). Measurement of Internal pH in *Helicobacter pylori* by Using Green Fluorescent Protein Fluorimetry. *Journal of Bacteriology*, 200(14), e00178-18.
51. Minamino, T., Imae, Y., Oosawa, F., Kobayashi, Y., Oosawa, K. (2003). Effect of intracellular pH on rotational speed of bacterial flagellar motors. *Journal of Bacteriology*, 185(4), 1190–1194.
52. Kihara, M., Macnab, R. M. (1981). Cytoplasmic pH mediates pH taxis and weak-acid repellent taxis of bacteria. *Journal of Bacteriology*, 145(3), 1209–1221.
53. Nakamura, S., Kami-ike, N., Yokota, J. ichi P., Kudo, S., Minamino, T., Namba, K. (2009). Effect of intracellular pH on the torque-speed relationship of bacterial proton-driven flagellar motor. *Molecular Biology*, 386(2), 332–338.
54. Khan, S., Macnab, R. M. (1980). The steady-state counterclockwise/clockwise ratio of bacterial flagellar motors is regulated by protonmotive force. *Molecular Biology*, 138(3), 563–597.
55. Sachs, G., Meyer-Rosberg, K., Scott, D. R., Melchers, K. (1996). Acid, protons and *Helicobacter pylori*. *The Yale Journal of Biology and Medicine*, 69(3), 301–316.
56. Qin, Z., Lin, W. T., Zhu, S., Franco, A. T., Liu, J. (2017). Imaging the motility and chemotaxis machineries in *Helicobacter pylori* by cryo-electron tomography.

- Journal of Bacteriology*, 199(3), e00695-16.
57. Chaban, B., Coleman, I., Beeby, M. (2018). Evolution of higher torque in Campylobacter-type bacterial flagellar motors. *Scientific Reports*, 8(1), 97.
 58. Wagner, C. E., Turner, B. S., Rubinstein, M., McKinley, G. H., Ribbeck, K. (2017). A Rheological Study of the Association and Dynamics of MUC5AC Gels. *Biomacromolecules*, 18(11), 3654–3664.
 59. Bansil, R., Hardcastle, J., Constantino, M. (2015). Microrheology of mucin : tracking particles and *Helicobacter pylori* bacteria. *Journal of Composite Materials*, 67(4), 150–154.
 60. Magariyama, Y., Sugiyama, S., Muramoto, K., Kawagishi, I., Imae, Y., Kudo, S. (1995). Simultaneous measurement of bacterial flagellar rotation rate and swimming speed. *Biophysical Journal*, 69(5), 2154–2162.
 61. Su, C., Padra, M., Constantino, M. A., Sharba, S., Thorell, A., Lindén, S. K., Bansil, R. (2018). Influence of the viscosity of healthy and diseased human mucins on the motility of *Helicobacter pylori*. *Scientific Reports*, 8(1), 9710.
 62. Bhaskar, K. R., Gong, D. H. , Bansil, R., Pajevic, S., Hamilton, J. A., Turner, B. S., LaMont, J. T. (1991). Profound increase in viscosity and aggregation of pig gastric mucin at low pH. *American Journal of Physiology-Gastrointestinal and Liver Physiology*, 261(5 Pt 1), G827–G832
 63. Rich, J. P., McKinley, G. H., Doyle, P. S. (2011). Size dependence of microprobe dynamics during gelation of a discotic colloidal clay. *Journal of Rheology*, 55(2), 273–299.

64. Lee, A. Y., Kao, C. Y., Wang, Y. K., Lin, S. Y., Lai, T. Y., Sheu, B. S., Lo, C. J., Wu, J. J. (2017). Inactivation of ferric uptake regulator (Fur) attenuates *Helicobacter pylori* J99 motility by disturbing the flagellar motor switch and autoinducer-2 production. *Helicobacter*, 22(4), 1–9.
65. Clyne, M., Labigne, A., Drumm, B. (1995). *Helicobacter pylori* requires an acidic environment to survive in the presence of urea. *Infection and Immunity*, 63(5), 1669–1673.
66. Rektorschek, M., Weeks, D., Sachs, G., Melchers, K. (1998). Influence of pH on metabolism and urease activity of *Helicobacter pylori*. *Gastroenterology*, 115(13), 628–641.
67. Fung, C., Tan, S., Nakajima, M., Skoog, E. C., Camarillo-Guerrero, L. F., Klein, J. A., ... Amieva, M. R. (2019). High-resolution mapping reveals that microniches in the gastric glands control *Helicobacter pylori* colonization of the stomach. *PLoS Biology*, 17(5), e3000231.
68. Pande, J., Merchant, L., Krüger, T., Harting, J., Smith, A. (2017). Setting the pace of microswimmers: when increasing viscosity speeds up self-propulsion based on morphological adaptations. *New Journal of Physics*, 19, 053024.
69. Tipping, M. J., Delalez, N. J., Lim, R., Berry, R. M., Armitage, J. P. (2013). Load-dependent assembly of the bacterial flagellar motor. *Molecular Biology*, 4(4), 1–6.
70. Lele, P. P., Hosu, B. G., Berg, H. C. (2013). Dynamics of mechanosensing in the bacterial flagellar motor. *Proceedings of the National Academy of Sciences of the United States of America*, 110(29), 11839–11844.

71. Son, K., Guasto, J. S. Stocker, R. (2013). Bacteria can exploit a flagellar buckling instability to change direction. *Nature Physics*. 7(9), 494–498.

CURRICULUM VITAE

